HHS Public Access

Author manuscript

*Cancer Res*. Author manuscript; available in PMC 2023 March 16.

# Pharmacological targeting of TFIIH suppresses KRAS mutant pancreatic ductal adenocarcinoma and synergizes with TRAIL

**Russell Moser**[1], **James Annis**[2], **Olga Nikolova**[3], **Clifford J Whatcott**[4], **Kay E Gurley**[1], **Eduardo Mendez**[1], **Kim Moran-Jones**[5], **Craig Dorrell**[6], **Rosalie C Sears**[6], **Calvin J Kuo**[7], **Haiyong Han**[8], **Andrew V Biankin**[5], **Carla Grandori**[9], **Daniel D Von Hoff**[10], **Christopher J Kemp**[11]

[1]Fred Hutchinson Cancer Research Center, Seattle, WA, United States.

[2]Institute for Stem Cell and Regenerative Medicine, Seattle, WA, United States.

[3]Oregon Health & Science University, Portland, OR, United States.

[4]Sumitomo Pharma Oncology, Lehi, United States.

[5]University of Glasgow, Glasgow, United Kingdom.

[6]Oregon Health & Science University, Portland, Oregon, United States.

[7]Stanford University, Stanford, CA, United States.

[8]Translational Genomics Research Institute, Phoenix, AZ, United States.

[9]Cure First and SEngine Precision Medicine, Seattle, WA, United States.

[10]TGen, Phoenix, AZ, United States.

[11]Fred Hutchinson Cancer Research Center, DC, WA, United States.

## Abstract

Pancreatic ductal adenocarcinoma (PDAC) typically presents as metastatic disease at diagnosis and remains refractory to treatment. Next generation sequencing efforts have described the genomic landscape, classified molecular subtypes, and confirmed frequent alterations in major driver genes, with coexistent alterations in KRAS and TP53 correlating with the highest metastatic burden and poorest outcomes. However, translating this information to guide therapy remains a challenge. By integrating genomic analysis with an arrayed RNAi druggable genome screen and drug profiling of a KRAS/TP53 mutant PDAC cell line derived from a patient-derived xenograft (PDCL), we identified numerous targetable vulnerabilities that reveal both known and novel functional aspects of pancreatic cancer biology. A dependence on the general transcription and DNA repair factor TFIIH complex, particularly the XPB subunit and the CAK complex

[b]To whom correspondence should be addressed.: Christopher J. Kemp, Fred Hutchinson Cancer Research Center, Division of Human Biology C1-015, 1100 Fairview Avenue NW, Seattle, WA 98109, cjkemp@fhcrc.org, Telephone: 206-667-4252.

[*]Present Address: Sumitomo Dainippon Pharma Oncology. 3900 N Traverse Mountain Blvd, Suite 100, Lehi, UT 84043

[a]Author is deceased.

**Author Contributions**. R.M., J.A., E.M., H.H., C.G., D.V.H., and C.J.K. designed research; R.M., J.A., C.W., K.G., K.M.J., H.H., C.D. performed research; C.G., D.V.H., C.J.K. supervised the study; R.C.S., C.K. H.H., D.V.H., K.M.J., A.B. provided reagents; R.M., J.A., O.N., C.W., K.M.J., E.M., C.J.K. analyzed data; R.M., D.V.H., and C.J.K. wrote the paper

Conflict of Interest Statements: The authors declare no potential conflicts of interest.

(CDK7/CyclinH/MAT1), was identified and further validated utilizing a panel of genomically subtyped KRAS mutant PDCLs. TFIIH function was inhibited with a covalent inhibitor of CDK7/12/13 (THZ1), a CDK7/CDK9 kinase inhibitor (SNS-032), and a covalent inhibitor of XPB (Triptolide), which led to disruption of the protein stability of the RNA polymerase II subunit RPB1. Loss of RPB1 following TFIIH inhibition led to downregulation of key transcriptional effectors of KRAS mutant signaling and negative regulators of apoptosis, including MCL1, XIAP, and CFLAR, initiating caspase-8 dependent apoptosis. All three drugs exhibited synergy in combination with a multivalent TNF-related apoptosis inducing ligand (TRAIL), effectively reinforcing mitochondrial-mediated apoptosis. These findings present a novel combination therapy with direct translational implications for current clinical trials on metastatic pancreatic cancer patients.

**Keywords**

functional genomics; TFIIH; transcriptional kinases; pancreatic ductal adenocarcinoma

## Introduction

PDAC is the third leading cause of cancer death in the United States, and the current 5-year survival rate for all patients diagnosed with pancreatic cancer is 8 percent (1). Surgical resection offers the best hope for long-term survival with a 17 percent survival rate, and while current first-line radiotherapy and chemotherapeutic regimens with gemcitabine plus nab-paclitaxel, and Folfirinox provide benefits, patients typically succumb to this disease within 1 year of diagnosis (2–6). Approximately, 80% of PDAC patients have regional and distant metastasis at time of diagnosis (1), and once detectable, clinical progression is extremely rapid (7). Signature genomic alterations in *KRAS*, *TP53*, *CDKN2A*, and *SMAD4* are associated with metastatic dissemination and a poor prognosis (8–10). Given the lack of major improvements in the clinical outcome of PDAC over the past five decades, innovative approaches are clearly called for to discover and develop novel therapeutic targets (11).

Genomic sequencing efforts on PDAC have revealed a complex mutational landscape, confirmed the high prevalence of mutations in the *KRAS* oncogene (91%), and *TP53* (61%), *CDKN2A* (27%), and *SMAD4* (28%) tumor suppressors with the majority of genomic alterations in KRAS co-occurring with TP53, and defined four pancreatic cancer subtypes based on structural genomic variation (SV subtype-Stable, Focal, Scattered, Unstable) (12). Transcriptional studies have defined two distinct primary lineage molecular subtypes, namely, classical pancreatic and squamous (13). While these biologically based classifications of pancreatic cancer are associated with outcome, and numerous clinical trials based on genomic and molecular features have been performed on other cancer types, clinical management for the majority of pancreatic cancer patients is not currently guided by this information (14).

Historically, targeting the KRAS mutant oncogene directly has proven difficult, but recent efforts have led to the first-in-human trial and FDA approval of sotorasib, a covalent inhibitor that binds the mutated cysteine residue, for patients with KRAS G12C-driven

non-small cell lung cancer (NCT04933695). Unfortunately, since PDAC patients almost exclusively harbor KRAS G12D/G12V mutations the efficacy of this targeted therapy is limited, and efforts have primarily focused on targeting downstream signaling (i.e., RAF-MEK-ERK) with MEK inhibitors in combination chemotherapy regimens (NCT01016483, NCT01251640). Previous studies have demonstrated that transcription factors STAT3, FOSL1, and MYC are important mediators of KRAS signaling and "drive" major elements of pancreatic cancer biology including progression, invasion, metastasis, and stromal remodeling *in vivo* (15–22). However, these transcription factors are challenging to target with small molecules. TP53, a key regulator of intrinsic apoptosis, is not currently druggable in its mutant form, but targeting underlying genomic instability and the DNA damage response (DDR) may have promise (23). For example, an inhibitor to the WEE1 kinase, in the context of locally-focused radiotherapy has recently been shown to increase progression-free survival in combination chemotherapy regimens in pancreatic cancer patients (24). Recently, a small subgroup of patients with metastatic disease and germline mutations in BRCA 1/2 (i.e., DDR-deficient), showed improved progression-free survival upon treatment with the PARP inhibitor Olaparib in a maintenance therapy regimen (POLO Study) (NCT02184195), suggesting a group of patients may benefit from genome guided therapy (25). These examples illustrate how patient selection and novel targeted agents, in clinical context with current therapy, may benefit patients. However, systemic and combination strategies to effectively treat most PDAC patients will depend on a more thorough understanding of the targetable vulnerabilities engendered in the context of signature genomic alterations in *KRAS, TP53, CDKN2A*, and *SMAD4*.

In this study, we demonstrate the application of a functional precision medicine approach (26,27) on a patient derived PDAC culture to identify therapeutic targets and potentially effective drugs. By integrating genomic analysis with high throughput genome-scale RNAi and drug profiling we generated a comprehensive map of targetable vulnerabilities and associated druggable signaling nodes. Subsequent functional genetic and drug profiling of these targets on a panel of genomically characterized KRAS mutant PDX PDAC cell lines (PDCLs) confirmed the efficacy of known targets and drugs, and revealed a dependency of KRAS mutant PDAC on the CDK7 transcriptional kinase, and the XPB (ERCC3) subunit of the general transcription and DNA repair factor TFIIH, essential for RNA polymerase II transcription. We show that TFIIH inhibition with the covalent CDK7/12/13 inhibitor THZ1, the CDK7/9 inhibitor SNS-032, and a covalent XPB inhibitor Triptolide, downregulate the expression of known transcriptional effectors of KRAS mutant signaling, STAT3 and FOSL1. We demonstrate that TFIIH inhibitors disrupt the protein stability of the RNA polymerase II Subunit B1 (RPB1), the largest subunit of RNA polymerase II, resulting in the downregulation of the CASP and FADD-Like Apoptosis Regulator, CFLAR, and critical inhibitors of apoptosis (IAPs), MCL1 and XIAP, to initiate a caspase-8 dependent apoptosis specifically in KRAS mutant PDCLs. We demonstrate that these TFIIH inhibitors in combination with a multivalent TNF-related apoptosis inducing ligand (TRAIL) exhibit a synergistic effect *in vitro*, essentially amplifying a programmed cell death response in a panel of KRAS mutant PDCLs, and suggest a novel combination strategy that could have direct translational implications on current clinical trials in PDAC patients.

## Materials and Methods

### Human research ethical approvals

The authors acknowledge that all research studies utilizing human specimens have been performed in accordance with the principles stated in the Declaration of Helsinki, and ethical approval has been obtained for all protocols from an Institutional Review Board (IRB) and/or ethics committee to meet national and international guidelines for human research.

### Cell Culture - Patient-derived cell line PancVH1 and HPNE

A surgical pancreatic tumor specimen was obtained during a pancreaticoduodenectomy (Whipple procedure) performed on a 75-year-old female patient diagnosed with pancreatic adenocarcinoma (histology grade 3) and a patient-derived xenograft (PDX) mouse model was generated, and a low-passage cell culture was isolated at Translational Genomics Research Institute (TGEN). Patient data and tissue were obtained with written informed consent in accordance with the Declaration of Helsinki and were acquired through the Biospecimen Repository Core of a Program Project (P01 CA109552) at TGEN under the Western Institutional Review Board (WIRB) protocol #20040832. This pancreatic adenocarcinoma low-passage cell culture (PancVH1) was established and propagated in growth medium including RPMI1640 (30-2001 ATCC), ITS supplement (354351-Corning): insulin (5μg/ml), transferrin (5μg/ml), selenium (5ng/ml), IGF-I (10ng/ml) (PHG0071-ThermoFisher Scientific), IGF-II (10ng/ml) (PHG0084 ThermoFisher Scientific), 10% fetal bovine serum (Atlas Biologicals). HPNE (CRL-4023), an hTERT-immortalized normal pancreas ductal epithelial cell line was obtained from ATCC as a non-tumorigenic control, and propagated in base medium that is 75% DMEM (D5030 Sigma), 2 mM L-glutamine (25030-081 ThermoFisher Scientific), 1.5 g/L sodium bicarbonate (25080-094 ThermoFisher Scientific), and 25% Medium M3 Base (M300F500 InCell Corp.), 5% fetal bovine serum, 10ng/ml human recombinant EGF (PHG0311L-Gibco), 5.5 mM D-glucose (1g/L) (G7021 Sigma), 750 ng/ml puromycin (P8833 Sigma).

### Patient-derived cell lines (PDCLs) from The Kinghorn Cancer Center

The PDX-derived primary cell lines (PDCLs), named The Kinghorn Cancer Center (TKCC) cell lines were generated in the laboratory as part of the Australian Pancreatic Cancer Genome Initiative - International Cancer Genome Consortium (ICGC) (12). All human research ethical approvals were granted and written informed consent of patients obtained in accordance with the Declaration of Helsinki and a ICGC approved process. Fourteen TKCC cultures were cultured: TKCC-02 was propagated in RPMI media: RPMI1640 (30-2001 ATCC), 10% FBS, 20 ng/ml EGF (PHG0311L-Gibco) and Primocin (Cat. ant-pm-1-InvivoGen). TKCC-05 and TKCC-06 were propagated in HPACmod media: DMEM/F12 (11320-033 – ThermoFisher Scientific), 15mM HEPES (15630-106- ThermoFisher Scientific), 8% FBS (Atlas Biologicals), 10ng/ml EGF (PHG0311L- Gibco), 40 ng/ml hydrocortisone (H0888 Sigma), Insulin (0.1 IU/ml) (12585-014 –ThermoFisher Scientific), 0.12% glucose (G8644 Sigma), 100 μg/ml Primocin and Gentamycin (15750-060 -ThermoFisher Scientific). TKCC-09, TKCC-10, TKCC-12, TKCC-14, TKCC-15-LO, TKCC-16-LO, TKCC-17-LO, and TKCC-27-LO were propagated in M199/F12 media:

M199/F12 (1:1) (11150-059/11765-054 ThermoFisher Scientific), 15 mM HEPES, 2mM glutamine (25030-081 ThermoFisher Scientific), 20 ng/ml EGF, 40 ng/ml hydrocortisone, Insulin (0.1 IU/ml), 5 μg/ml apo-transferrin (T1147 Sigma), 0.06% glucose, 7.5% FBS, 0.5 pg/ml tri-iodotyronine (T6397-Sigma), MEM vitamins (11120-052 ThermoFisher Scientific), 2 μg/ml O-phosphoryl-ethanolamine (P0503 Sigma), 100 μg/ml Primocin and Gentamycin. TKCC-18-LO, TKCC-19-LO, TKCC-22-LO were propagated in IMDMrich media: IMDM (12440-053 ThermoFisher Scientific), 20% FBS, 20 ng/ml EGF, 2.5 μg/ml apo-transferrin, Insulin (0.2 IU/ml), 0.5x MEM vitamins, 100 μg/ml Primocin and Gentamycin. TKCC cultures designated with the label (LO) were propagated in low-oxygen incubators at 37°C in 5%O2, while all additional TKCC cultures were propagated in incubators at 37°C with 5% $CO_2$ in air. Waddell et al. 2015 utilized whole-genome sequencing (WGS) and copy number variation (CNV) data on 99 patient samples to identify somatic structural variants (qSV tool), and classify pancreatic cancer samples into 4 subtypes according to the frequency and distribution in somatic variation of the genome: *Stable* - tumors that contain few structural rearrangements (<50) which are located randomly through the genome, *Focal (locally rearranged)* - The intra-chromosomal rearrangements in these tumors are not randomly positioned through the genome, instead they are clustered on one or few chromosomes, *Scattered* - These tumors contain 50–200 structural rearrangements which are scattered throughout the genome, *Unstable* - These tumors are massively rearranged as they contain > 200 structural rearrangements which are scattered throughout the genome (12,28). PDX mouse models were generated from a subset of these samples and propagated, and TKCC PDX derived lines (PDCLs) were isolated and established. Cross reference of patient samples (ICGC number), and corresponding isolated TKCC PDCL with structural variant subtype (SV subtype) classification for all 14 lines is shown. TKCC PDCL molecular subtype is also noted with two distinct primary lineages, classical pancreatic (orange), and squamous (blue). It should be noted that of the 14 TKCC PDCLs, only one representative line is classified as classical pancreatic (TKCC-22-LO), and nine TKCC PDCLs classified as squamous, and four TKCC PDCLs unclassified.

## Whole exome sequencing

DNA was isolated from both PancVH1 cell culture and peripheral blood mononuclear cells (PBMC) from the same patient as a normal reference control utilizing the Wizard SV Genomic Purification Kit (Promega). Quantity of double stranded DNA was determined by Quant-iT™ PicoGreen® dsDNA Assay Kit (P11496 Thermo Fisher Scientific). Whole exome sequencing was performed at the University of Washington Northwest Genomics Center (NWGC) (http://nwgc.gs.washington.edu/) using the Nimblegen SeqCap probes on an Illumina platform. WES-Variant Annotation. We used an automated pipeline for annotation of variants derived from exome data, the SeattleSeq Annotation Server 137 (http://snp.gs.washington.edu/SeattleSeqAnnotation137/). This publicly accessible server returns annotations including dbSNP rsID (or whether the coding variant is novel), gene names and accession numbers, predicted functional effect (e.g., splice-site, nonsynonymous, missense, etc.), protein positions and amino-acid changes, PolyPhen predictions, conservation scores (e.g., PhastCons, GERP), ancestral allele, dbSNP allele frequencies and known clinical associations. The annotation process has also been automated into our analysis pipeline to produce a standardized, formatted output (VCF-

variant call format, described above). Variant calls and annotation were also generated using VarScan (v2.3.6) (29) and MuTect (v1.1.4) (30) with default parameter settings. SNP and indel calls were generated in reference to human genome build hg19 (SI Dataset S1).

### Array comparative genomic hybridization (aCGH)

DNA was isolated from PancVH1 and aCGH was performed as previously described (31), $\log_2$ratio > 0.584, and $\log_2$ratio < −1.0 was used to call gene level amplifications and deletions, respectively. Gene level amplifications (amplicons) were cross referenced to PancVH1 Druggable Genome RNAi Screen (FDR<0.3); (SI Dataset S1).

### Arrayed druggable genome RNAi screen on patient-derived cell line PancVH1

The MISSION® Human Druggable Genome siRNA library (SI00100 Sigma) consists of three distinct siRNAs per gene targeting 6,659 genes. The human druggable genome siRNA working library was constructed and arrayed in a 384-well format with pools of the three independent siRNAs targeting each gene, in a one gene per well approach. A druggable genome RNAi screen was performed on PancVH1 at University of Washington Quellos High-Throughput Screening Core facility utilizing an array-based siRNA screening platform (https://iscrm.uw.edu/research/core-resources/quellos-high-throughput-screening-core/). PancVH1 cells were arrayed in 384-well plates in 50μl per well of complete medium using a Matrix WellMate Dispenser (ThermoFisher Scientific) and cultured for 24 hours at 37°C in a 5%CO2 incubator. Liposomal siRNA complexes were generated using Lipofectamine RNAiMAX Reagent (13778500 ThermoFisher Scientific) and Opti-MEM (31985-062 Thermo Scientific), with three siRNAs targeting the same gene pooled at equal molarities and the druggable siRNA library arrayed/transfected in triplicate in independent plates with the CyBio CyBi-Well Vario Liquid Handler (CyBio, Germany). Pancreatic cell cultures/siRNA liposomal complexes were incubated at 37°C in a 5% CO2 incubator for 96 hours and cell viability was measured as a phenotypic endpoint using the CellTiterGlo assay (Promega) and raw luminescence detected and quantified with an Envision Multilabel plate reader (PerkinElmer). Raw luminescence signal was mock normalized per plate to calculate the percent viabilities for each gene and a library-based homoscedastic t-test p-value was computed. Replicate signals were summarized into a mean value, Z-transformed and plotted for distribution and data mining using a negative control siRNA (non-targeting siRNA) and a positive control siRNA targeting the motor protein, kinesin family member 11 (KIF11). Statistical analysis of the druggable genome RNAi screen was performed utilizing both library-based and plate-based median absolute deviation (MAD) to generate high confidence hit calls (32,33). Library-based and plate-based metrics were used to select 327 high confidence targets (327/6659 – 5%) for validation. RNAi screen metrics and selection criteria of targets: library based (Zscore, q-value (FDR)), and plate-based (MAD) to select High Confidence siRNA hits: (1) FDR <0.15, MAD >2 (All 3 siRNA replicates scoring positive) - MAD set at 95% Kif11 (Positive control); (2) PancVH1 Somatic Mutations (FDR<0.3); (3) PancVH1 CGH Amplifications (FDR<0.3, MAD>1); (4) Cross reference of PancVH1 screen with top 298 gene target mean rank differentials from 7 KRAS mutant JHU PDAC cell line extended kinome screens vs. HPNE (FDR<0.3); (5) Drug Availability Prioritization – Ingenuity Pathway Analysis (FDR<0.3); (6) TCGA (cBioPortal) mutation frequency > 5% (FDR <0.3, MAD>1); (7) PDAC Cherry

Pick (FDR<0.3). Pancreatic pathway internal controls KRAS, TP53, CDKN2A, SMAD4 (Gene Solution Qiagen) and pancreatic-pathway genes (46 genes Qiagen) were also included as spike-in siRNAs for biological context (SI Dataset S2). Data is deposited in CTD$^2$ Dataportal - functional exploration of the druggable genome in pancreatic ductal adenocarcinoma (https://ocg.cancer.gov/programs/ctd2/data-portal)).

### Arrayed RNAi extended kinome screens on PDAC cell lines and HPNE

The MISSION® Human Kinome siRNA library (Sigma) consists of three siRNAs per gene targeting (713 genes) kinases. The human kinome siRNA working library was constructed and arrayed in a 384-well format with pools of the three independent siRNAs targeting each gene, in a one gene per well approach. We also designed a custom KempMoser Pancreatic OncoLibrary (267 genes) consisting of a pancreatic-specific oncolibrary [pancreatic-specific biomarkers (81 genes) (34), pancreatic-specific extracellular/membrane associated genes from SAGE expression analysis (44 genes) (9), pro- and anti-apoptotic and autophagic genes (90 genes), pancreatic pathway controls (46 genes), and select chromatin modifying enzymes (6 genes)], and a DNA damage and repair (DDR) library (318 genes) were also added to this kinome screen (SI Dataset S3). Data is deposited in CTD$^2$ Dataportal - functional exploration of the kinome in pancreatic ductal adenocarcinoma (https://ocg.cancer.gov/programs/ctd2/data-portal)). RNA interference (RNAi) extended kinome screens were performed utilizing an array-based siRNA platform on seven PDAC cell lines: Johns Hopkins University (JHU) set including Panc02.03 (CRL-2553), Panc03.27 (CRL-2549), Panc04.03 (CRL-2555), Panc05.04 (CRL-2557), Panc08.13 (CRL-2551), PancPL45 (CRL-2558), Panc10.05 (CRL-2547)] (35), and HPNE (CRL-4023) an hTERT immortalized normal pancreas ductal epithelial cell line obtained from ATCC (36). RNAi extended kinome screens were performed in 384-well format in triplicate, in independent plates, utilizing robotics instrumentation. PDAC and HPNE cell lines were plated in 384-well plates in 50μl per well of complete medium using a WellMate (Matrix Technologies, Canada) and transfected with siRNAs 24 hours later using Lipofectamine RNAiMAX Reagent (ThermoFisher Scientific, MA, USA), with three siRNAs targeting the same gene pooled at equal molarities. Plates were incubated at 37°C in a 5% CO2 incubator for 72–96 hours and cell viability was measured as a phenotypic endpoint using the CellTiterGlo assay (Promega) and raw luminescence detected and quantified with an Envision Multilabel plate reader (PerkinElmer). Raw luminescence values were mock normalized per plate and plotted for distribution and data mining using a negative control siRNA (non-targeting siRNA) and a positive control siRNA targeting the motor protein, kinesin family member 11 (KIF11). Methods of analysis of RNAi screens were performed as previously described (26,32). Mean rank differential analysis was performed with library-based Z-scores of RNAi gene targets for each of 7 KRAS mutant PDAC cell lines and rank differentials were generated versus the HPNE cell line with 298 targets with mean rank differentials greater than the KRAS gene target (SI Dataset S3). Top mean rank differentials (298 gene targets) were cross-referenced to select RNAi gene targets from the druggable genome RNAi screen (criteria for selection).

### Arrayed secondary RNAi screen on patient-derived cell line PancVH1 and HPNE

Library-based and plate-based metrics were used to select 327 high confidence ‘hits’ (327/6659 – 5%) for validation from the druggable genome RNAi screen (SI Dataset

S3). A custom RNAi secondary library was designed, constructed, and arrayed utilizing independent pools (3 siRNAs/gene) ordered from Qiagen in a Flexiplate siRNA format (1027422). A secondary RNAi screen was performed in a 384-well format as above but in quadruplicate on both PancVH1 and HPNE cells. Briefly, PancVH1 and HPNE cells were arrayed in 384-well plates in 50μl per well of complete medium using a Matrix WellMate Dispenser (ThermoFisher Scientific) and cultured for 24 hours at 37°C in 5%CO2 incubator. Liposomal siRNA complexes were generated using Lipofectamine RNAiMAX Reagent (13778500 ThermoFisher Scientific) and Opti-MEM (31985-062 Thermo Scientific), with three siRNAs targeting the same gene pooled at equal molarities and the small-scale siRNA library arrayed/transfected in quadruplicate in independent plates with the CyBio CyBi-Well Vario Liquid Handler (CyBio, Germany). Cells/siRNA liposomal complexes were incubated at 37°C in a 5% CO2 incubator for 96 hours and cell viability was measured as a phenotypic endpoint using the CellTiterGlo assay (Promega) and raw luminescence detected and quantified with an Envision Multilabel plate reader (PerkinElmer). Cellular viabilities were calculated using raw luminescence values normalized to the mock condition on a per plate basis and plotted for distribution and data mining using a negative control siRNA (non-targeting siRNA). Statistically significant 'hits' were determined via unpaired two-tailed t-test vs. negative control siRNA condition with $-\log_{10}$P-value >1 deemed significant. Rank differential analysis was performed as above on PancVH1 and HPNE secondary screen results and targets prioritized by cross reference to mean rank differentials (298 gene targets) from the arrayed RNAi extended kinome screens (SI Dataset S3).

### Molecular Signatures Database (MSigDB)

For geneset identification, the hypergeometric overlap statistic tool was used to calculate the overlap between significant candidate RNAi gene targets ($-\log_{10}$P-value >1) and pathways in MSigDB v6.2 (Molecular Signatures Database) (http://software.broadinstitute.org/gsea/msigdb/annotate.jsp) (37); significant pathways defined as FDR<0.05 (SI Dataset S3).

### Confirmation of CDK-activating kinase (CAK) complex both in PancVH1 and HPNE

Biochemical purification of the CAK complex in PancVH1 and HPNE was performed via immunoprecipitation (IP) and immunoblotting (IB) with antibodies to CDK7 (2916), Cyclin H (2927), Mat1 (sc-135981), and Protein A/G PLUS-Agarose (sc-2003 Santa Cruz) via standard protocol.

### Gene target validation of CAK complex (CDK7, Cyclin H) and CFLAR in PancVH1 and HPNE

PancVH1 and HPNE cells were seeded at $3 \times 10^3$ per/well (80μl) in a 96-well plate and incubated at 37°/5% $CO_2$ for 12–18 hours. TriFECTa dsiRNAs for CFLAR (hs.Ri.CFLAR.13.1–13.3), CDK7 (hs.Ri.CDK7.13.1–13.3), and Cyclin H (hs.Ri.CCNH.13.1–13.3) with negative control dsiRNA duplex (NC1) (Integrated DNA Technologies), and AllStars Hs Cell Death (siDeath) positive control (SI04381048 Qiagen) were used per manufacturers protocol with pooled dsiRNAs and individual dsiRNA per gene target showing the largest phenotypic effect via colony assay (see below) and on-target effect via immunoblot (see below). Cells were transfected with liposomal dsiRNA/siRNA complexes in Opti-MEM (20μl/well) resulting in a final concentration of 10nM (0.05μl

of 20μM dsiRNA/well) / Lipofectamine RNAiMax (0.2μl/well). All transfections were performed in triplicate with pooled dsiRNA, individual dsiRNAs per target with negative (NC_dsiRNA) and positive controls (AllStars siDeath or siDeath). Cell viability at 96 hrs post-transfection was measured using the CellTiterGlo luminescence assay (Promega) and the Synergy H4 (Biotek). Raw luminescence signal was normalized to mean negative control dsiRNA (NC_dsiRNA) per transfection condition, and statistical significance ($P<0.05$) was assessed via unpaired two-tailed t-tests vs. NC_dsiRNA condition. Differential viabilities were calculated for each dsiRNA knockdown (CDK7, CCNH), and CFLAR between PancVH1 and HPNE and an unpaired two-tailed t-test was utilized to determine significant selective dependency of gene target knockdown.

### DsiRNA gene target validation in PDCLs

TriFECTa dsiRNA kits for CFLAR (hs.Ri.CFLAR.13.1–13.3), CDK7 (hs.Ri.CDK7.13.1–13.3), Cyclin H (hs.Ri.CCNH.13.1–13.3), CDK13 (hs.Ri.CDK13.13.1–13.3), CDK9 (hs.Ri.CDK9.13.1–13.3), and XPB (hs.Ri.ERCC3.13.1–13.3) with negative control dsiRNA duplex (NC1) (Integrated DNA Technologies), and AllStars Hs Cell Death (AllStars siDeath) positive control (SI04381048 Qiagen) included in all experiments to assess phenotypic endpoints and quality of transfection. A colony assay was utilized to assess individual dsiRNAs (n=3) per gene target: CDK7, CCNH, CFLAR, CDK13, CDK9, XPB on cellular viability in PancVH1. PancVH1 were plated at $2 \times 10^4$ cells per well in 12-well plates, 25nM dsiRNAs were transfected with Lipofectamine RNAiMax at 24 hours and plates were incubated at 37°/5% $CO_2$ for 7 days, washed with PBS, and stained for 10 minutes with crystal violet dye (125mg dye/50ml Methanol(20%)/H20), rinse, and imaged. dsiRNA engagement of target was assessed by protein target knockdown in PancVH1. Cells were transfected with 25nM negative control dsiRNA, pooled dsiRNAs, and individual dsiRNAs per target. Transfections were performed with $2 \times 10^5$ cells in 6-well plates for 24 hrs, cells were then washed with PBS, trypsinized, and reseeded in 60mm plates for 24 hrs and a second transfection was performed and protein extracts harvested at 48 hours. Protein extracts were quantitated using the BCA assay (ThermoFisher Scientific). Protein extracts were separated via PAGE, transferred to PVDF membrane, and immunoblotted. Protein knockdown of CFLAR, CDK7, Cyclin H, CDK13, CDK9, and XPB with dsiRNAs was confirmed with antibodies to CDK7 (2916), Cyclin H (2927), CFLAR (ALX-804-961 ENZO), CDK13 (ABE1860 Millipore), CDK9 (2316), and XPB(ERCC3) (8746). PDCLs (PancVH1, TKCC_02, TKCC_05, TKCC_06, TKCC_09, TKCC_15_LO, TKCC_16_LO, TKCC_17_LO, TKCC_18_LO, TKCC_27-LO) were used to validate knockdown efficacy on cellular viability for all six gene targets. Cells were transfected with liposomal dsiRNA/siRNA complexes in Opti-MEM (20μl/well) resulting in a final concentration of 25nM/Lipofectamine RNAiMax (0.2μl/well). All transfections were performed in sextuplicate (n=6) with pooled dsiRNAs and negative (-ve control) and positive control (+ve control). Cellular viability at 120 hrs post-transfection was measured using the CellTiterGlo luminescence assay (Promega) and the Synergy H4 (Biotek). Raw luminescence signal was normalized to mean negative control dsiRNA (-ve control) per transfection condition, and statistical significance was assessed via one-way ordinary ANOVA with Dunnett's post-test for multiple comparisons vs. negative control (-ve control) dsiRNA condition.

### Drug profiling with CTD$^2$ Network Informer Set (CNIS) library

PancVH1 cells were propagated in growth medium including RPMI1640 (30-2001 ATCC), ITS supplement: insulin (5μg/ml), transferrin (5μg/ml), selenium (5ng/ml), IGF-I (10ng/ml), IGF-II (10ng/ml), 10% fetal bovine serum. HPNE (CRL-4023), an hTERT-immortalized normal pancreas ductal epithelial cell line obtained from ATCC as a non-tumorigenic control was propagated under ATCC conditions. High-throughput robotic drug screening was performed at the University of Washington Quellos High Throughput Screening Core (https://iscrm.uw.edu/research/core-resources/quellos-high-throughput-screening-core/). Briefly, $1\times10^3$ cells per line (PancVH1, HPNE) were plated in 384-well format in 50μl of complete medium per well using a WellMate (Matrix Technologies, Canada) and CTD2 320 informer set drug library was added 24 hours later with a CyBio Well Vario (Analytik Jena AG, Germany). All 320 drugs were tested in duplicate using a series of 10-point dilutions ranging from 0.5nM to 10μM. Cell cultures were propagated and drug profiling performed at 37°C in a 5% CO2-humidified incubator. Cell viability was quantified 72 hours after drug treatment using CellTiterGlo luminescence assay (Promega). Raw luminescence signals were normalized to vehicle control for each drug. Drug curves were fitted with XLfit (IDBS, Alameda, CA) utilizing a 4-parameter logistic dose response model; y = (Y min + (Y max/(1 + ((x/EC50)Slope)))) where Ymin is constrained from −2 >< 2, Ymax is constrained from 80><120, slope is constrained to >0.2; single site model. IC50, AUC, and R-squared were calculated for each compound (SI Dataset S4). Data is deposited in CTD$^2$ Dataportal (https://ocg.cancer.gov/programs/ctd2/data-portal)).

### Drug profiling of RNAi targets, RAS signaling/pancreatic cancer specific and epigenetic targets

Ingenuity Pathway Analysis (IPA) on the druggable genome RNAi library was utilized to select RNAi targets for further validation based on the availability of small molecule inhibitors (i.e., Drug Prioritization (FDR<0.3) see above and investigator curated) (SI Dataset S4). Dose response curves on both PancVH1 and HPNE were generated for select small molecule inhibitors in 96-well format singleton 10-point dilutions, and 384-well format quadruplicate,10-point dilutions ranging from 3nM - 100μM. Cell cultures were propagated and drug profiling performed at 37°C in a 5% CO2-humidified incubator. Cell viability was quantified 72 hours after drug treatment using CellTiterGlo luminescence assay (Promega). Raw luminescence signals were normalized to vehicle control for each drug. Drug curves were fitted with non-linear regression utilizing a 3-parameter logistic dose response model (Prism 7, GraphPad Software Inc.) and nplr package in R to generate IC50 and AUC-trapezoid method estimates for each compound. RNAi targets: Gemcitabine (S1149), SNS-032 (S1145), AZD1775 (S1525), AZD7762 (S1532), BYL719 (S2814), BMS536924 (S1012), OSI-906 (S1091), (5Z)-7-Oxozeaenol (3604 Tocris), AZ628 (S2746), PF-06465469 (4710 Tocris), Dabrafenib (S2807), GDC-0879 (S1104), Saracatinib (S1006), NVP-AEW541(S1034), LY441575 (S2714), Zoledronic acid monohydrate (SML0223 Sigma), Lonafarnib (S2797), Tadalafil (S1512), SB590885 (S2220), AZD4547(S2801), PF05263555 (WAY-399478 - Pfizer), Tofacitinib (S5001). RAS signaling/PDAC small molecule: Oncrasin-1 (3427 Tocris), Triptolide (3253 Tocris), Trametinib (A-1258 ActiveBiochem), Ibrutinib (S2680), ML281 (4880 Tocris), LDE225

(S2151), MRT 67307 (SML0702 Sigma), AZD2281 (S1060), ML323 (S7529), AG879 (2617 Tocris), Sorafenib (8705 Cell Signaling Technology), Celecoxib, (3786 Tocris), Arcyriaflavin A (2457 Tocris), Ganetespib (STA-9090) (S1159), PD173074 (S1264), Embelin (2156 Tocris). Epigenetic Tool Compounds: JQ1 (4499 Tocris), IOX1 (4464 Tocris), SGC-CBP30 (4889 Tocris), PFI-1 (4445 Tocris), EPZ6438 (S7128), I-CBP 112 (4891 Tocris), IOX2 (4451 Tocris), GSK343 (SML0766 Sigma), UNC1999 (SML0778 Sigma), SGC0946 (4541 Tocris), PFI-3 (SGC), GSK126 (S7061).

### TP53 Consensus Coding Sequence (CCDS) of variants in The Kinghorn Cancer Center (TKCC) PDCLs

TP53 consensus coding sequence (CCDS) of variants in the TKCC PDX PDAC cell cultures (PDCLs): TKCC-02, TKCC-05, TKCC- 06, TKCC-09, TKCC-10, TKCC-12, TKCC-14, TKCC-15-LO, TKCC-16-LO, TKCC-17-LO, TKCC-18-LO, TKCC-19-LO, TKCC-22-LO and TKCC-27-LO – Seshat (http://p53.fr/tp53-database/seshat) (SI Dataset S5).

### Drug profiling of The Kinghorn Cancer Center (TKCC) PDCLs

The 14 TKCC cell lines were propagated in their respective medias (see above) and dose response curves were generated with 22 select small molecule inhibitors in 96-well format with singleton 10-point dilutions ranging from 0.1pM - 100μM. Cell cultures were propagated and drug profiling performed at 37°C in a 5% CO2-humidified incubator. Cell viability was quantified 72 hours after drug treatment using CellTiterGlo luminescence assay (Promega). Raw luminescence signals were normalized to vehicle control for each drug. Drug curves were fitted with both non-linear regression utilizing a 3-parameter logistic dose response model (Prism Version 7 GraphPad Software Inc.), and the nplr package in R. IC50, and AUC estimates were calculated for each compound. TKCC Drug Profiling: Gemcitabine (S1149), Romidepsin (S3020), MK1775 (S1525), JQ1 (4499 Tocris), Cdk/Crk inhibitor (219491 EMD Millipore), BML-277 (BML-EI388 Enzo), THZ1 HCL (B4736 ApexBio), DASA-58(HY-19330 Medchem Express), Bortezomib (S1013), YM-155 (S1130), Bardoxolone Methyl (1772 Axon Medchem), Mitomycin C (S8146), FK866 (S2799), Erlotinib HCl (S1023), Trametinib (A-1258 ActiveBiochem), SNS-032 (S1145), SGC-CBP30 (4889 Tocris), PFI-1 (4445 Tocris), AZD7762 (S1532), Triptolide (3253 Tocris), BYL719 (S2814), BMS-536924 (S1012), OSI-906 (S1091), (5Z)-7-Oxozeaenol (3604 Tocris), AZ628 (S2746), PF-06465469 (4710 Tocris), GSK343 (SML0766 Sigma), and UNC1999 (SML0778 Sigma). Additional drug profiling was performed utilizing 11 TKCC cell lines propagated in their respective medias (see above) and dose response curves (8 drugs: THZ1, SNS-032, Triptolide, AZD1775, JQ1, Romidepsin, Bardoxolone Methyl, FK866) were generated with select small molecule inhibitors in 384-well format in quadruplicate with 10-point dilutions ranging from 1.5nM - 30μM. Cell cultures were propagated and drug profiling performed at 37°C in a 5% CO2-humidified incubator. Cell viability was quantified 72 hours after drug treatment using CellTiterGlo luminescence assay (Promega). Raw luminescence signals were normalized to vehicle control for each drug. Drug curves were fitted with non-linear regression utilizing a 3-parameter logistic dose response model (Prism Version 7 GraphPad Software Inc.) and nplr package in R to generate IC50, and AUC-trapezoid method estimates for each compound (SI Dataset S6).

### Immunoblotting and RAS-GTP Assay

Whole cell lysates for immunoblotting were prepared with RIPA buffer (50mM Tris pH 8.0, 150mM NaCl, 1% NP-40, 0.5% sodium deoxycholate, 0.1% SDS, 5mM EDTA) and/or Cell Lysis Buffer (Cell Signaling Technology 9803) with addition of both protease inhibitor cocktail (Roche Cat. No. 04 693 159 001) and phosphatase inhibitor cocktail (Roche Cat. No. 04 906 837 001). Whole cell lysates were collected and snap-frozen in liquid nitrogen before being stored at −80C. Protein concentrations were determined with BCA protein assay kit (Thermofisher Cat no. 23225). Protein extracts were loaded on NuPAGE 4%–12% and 12% Bis-Tris Mini Gels (Invitrogen, Carlsbad, CA) and separated by electrophoresis at 150 V for 2 hrs, and transferred onto PVDF membranes (Immobilon-FL Cat. No. IPFL00010, Millipore) and blocked by incubation with 5% non-fat dry milk in TBS. Membranes were probed using primary antibodies raised against the indicated proteins, and with appropriate near-infrared fluorescent secondary antibodies, and detected with the Odyssey CLx infrared imaging system (Li-COR Biosciences). For the RAS-GTP assay, GST-Raf1-RBD fusion protein was used to bind the activated form of GTP-bound Ras, immunoprecipitated with glutathione resin, and Ras activation levels determined by western blot with a Ras Mouse mAb as per manufacturer's protocol (Active Ras Detection Kit-Cell Signaling Technology). For immunoblotting, unless otherwise indicated, all antibodies listed with only catalog numbers were obtained from Cell Signaling Technology: CFLAR (ALX-804-961 ENZO), Rb (554136 BD Pharmingen), Caspase-8 (9746), Caspase-3 (9665), Mcl-1 (sc-12756), PARP (9542), XIAP (2042), Bcl-xL (2764), Cleaved Caspase-3 (9664), p53 Ab-5 (DO-7) (MS-186-P ThermoFisher Scientific, p53 (DO-7) (MA5-12557 Thermofisher Scientific), Phospho-Histone H2A.X (9718), Phospho-Rb (Ser608) (2181), p21 (556430 BD Pharmingen), c-MYC (61075-Active Motif), GAPDH (5174), cdc2 (CDK1) (9116), XPB (8746), XPD (11963), CDK2 (2546), Phospho-cdc2 (CDK1) (Thr161) (9114), Phospho-CDK2 (Thr160) (2561), Cleaved PARP (9546), Anti-RNA polymerase II subunit B1 (phospho-CTD Ser-2) clone 3E1 (04-1571-I Millipore), RNA pol II CTD phospho-Ser5 (61701-Active Motif), RPB1/Pol II (A-10) (sc-17798 Santa Cruz), TRAIL R1/TNFRSF10A (NB100-56747 Novusbio), TRAIL R2/TNFRSF10B (NB100-56618 Novusbio), MEK1/2 (4694), Phospho-MEK1/2 (Ser217/221) (9154), RAS (ab55391 Abcam), SMAD4 (sc-7966 Santa Cruz), AKT (pan) (4691), Beta-Actin (3598R-100 Biovision), STAT3 (9139), FOSL1 (5281), FOSL2 (19967), and E2F1 (3742). For immunoprecipitation and immunoblotting, CDK7 (2916), Cyclin H (2927), Mat1 (sc-135981), BID (2002), and Protein A/G PLUS-Agarose (sc-2003 Santa Cruz).

### Caspase-8 activity assay

PancVH1 and HPNE cells were plated in 96-well plates and allowed to grow to near confluency as per manufacturer's protocol CaspaseGlo-8 (Promega). Cell lines were treated with vehicle (DMSO) and 500nM THZ1, 500nM SNS-032, and 500nM Triptolide for 24 hrs in a 37°C incubator at 5%CO2 in air. Equal volumes of the CaspaseGlo-8 reagent were added to cells and mixed for 1hr on rotator, and luminescence signal measured utilizing a Synergy H4 (Biotek). Caspase-8 Inhibition Assay. PancVH1 and HPNE cells were plated in 96-well plates at 5×103 cells/well and incubated for 24 hrs at 37°C in 5%CO2. Cell lines were treated with vehicle (DMSO) and 500nM THZ1, 500nM SNS-032, and 500nM Triptolide with and without a cysteine protease/effector caspase inhibitor as a control (Z-

FA-FMK) (S7391 Selleckchem) and a specific caspase-8 inhibitor (Z-IETD-FMK) (S7314 Selleckchem) for 24 hrs in a 37°C incubator at 5%CO2 in air. Raw luminescence signals were measured with the CellTiterGlo assay (Promega) utilizing a Synergy H4 (Biotek).

### Cell cycle analysis

PancVH1 and HPNE cells were treated with DMSO (v/v) vehicle or 500nM THZ1 for 24, 48 and 72 hrs in a 37°C incubator at 5%$CO_2$. Cells were harvested and aliquoted at $1\times10^6$ cells per well in a 96-well round bottom plate, centrifuged at 400 × g (1500rpm), media decanted, and washed (3x) with 2%FCS/PBS (pH 7.2). Cells were then fixed and permeabilized (200μl/well) with ice-cold 70% ethanol and stored at −20°C until all time points were collected. Cells were subsequently centrifuged and washed/decanted (3X) with 2%FCS/PBS (pH 7.2), and stained with 50μg/ml propidium iodide (P4170 Sigma) in PBS (pH 7.2) with 100 μg/ml RNaseA for 3 hours at 4°C. Flow cytometric analysis was performed with the BD FACS Canto II (BD Biosciences) and at least 10,000 gated events were acquired per sample. Cell cycle analysis was performed using the FlowJo version 10 (FlowJo LLC).

### Bliss independence drug synergy assay

PDCLs - $3 \times 10^3$ cells/well were plated in a 6×6 matrix in a 96-well plate and incubated for 24 hours at 37°C in 5% CO2 in air. Drug curve serial dilutions were created for single drugs (THZ1, SNS-032, Triptolide), and izTRAIL (AG-40B-0069-C010 Adipogen) with ranges of concentrations covering the median effect of each agent, and vehicle (no drug) in a 2X format in complete media and applied to matrix layout of cells with single and combinations drug curves and incubated at 37°C in 5%$CO_2$ for 72 hours. Cell viability was then measured with CellTiterGlo assay (Promega) and raw luminescence was normalized to vehicle condition. Drug synergy was evaluated using the Bliss independence model (38). Briefly, the predicted fractional growth inhibition of the drug combination is calculated using the equation $F_A + F_B - (F_A \times F_B)$, where $F_A$ and $F_B$ are the fractional growth inhibitions of the individual drugs A and B at a given dose. Bliss excess is the difference between the expected growth inhibition and the observed inhibition from the drug combination. Bliss scores greater than zero, close to zero, and less than zero denote synergy, additivity, and antagonism, respectively. Bliss sum is the sum of individual Bliss scores in the 25-point (5 × 5) combination matrix of drug doses.

### TRAIL sensitivity assay

PDCLs and HPNE cells were seeded in 96-well plates at $3\times10^3$ cells/well and incubated at 37°C/5%CO2 for 24 hrs. Cells were treated with vehicle ($H_2O$) or TRAIL agonists (0–400 mg/ml): izTRAIL (AG-40B-0069-C010 Adipogen), and cell viability measured at 72 hours post-treatment with CellTiterGlo luminescence assay (Promega) and Synergy H4 (Biotek). Cell viabilities were calculated using raw luminescence signals normalized to vehicle condition. Fitted curves generated with non-linear regression in Prism 7 (Graphpad Software Inc.).

### Drug profiling of PDAC Patient-derived tumor organoids with the CTD$^2$ Network Informer Set (CNIS)

Pancreatic ductal adenocarcinoma patient-derived tumor organoids (PDTO: OPTR 3793 (ID 323793), OPTR 7021 (ID 357021), OPTR 3560 (ID 323560), OPTR 3578 (ID 323578)) were derived and sequenced at the Brenden-Colson Center for Pancreatic Care. Patient data and pancreatic tumor specimens recovered as surgical explants were obtained with written informed consent in accordance with the Declaration of Helsinki and were acquired through the Oregon Pancreas Tissue Registry (OPTR) under Oregon Health & Science University Institutional Review Board protocol #3609. PDTOs were propagated in Advanced DMEM/F12, 10mM HEPES (1M), B-27 (Gibco-17504044), N-2 (Gibco-17502048), 50 ng/ml huEGF (R&D Systems 236EG200), 50 ng/ml FGF10 (Peprotech 100–2), 10mM Nicotinamide (Sigma N0636), R-spondin conditioned media, 100 ng/ml huNoggin (StemRD NOGG-050), 100 ng/ml huWnt3A (R&D Systems 5036-WN), 1.25 mM N-acetyl-L-cysteine (Sigma A7250), 6 μM SB431542 (Tocris1614), Glutamax, Pen/Strep/Amphotericin, 1% Geltrex (ThermoFisher A1569601). High-throughput robotic drug screening was performed at the University of Washington Quellos High Throughput Screening Core (http://depts.washington.edu/iscrm/quellos/small-molecule-screens). Briefly, 1–2 × $10^3$ cells per line were plated in 384-well format in 50μl of complete medium per well using a WellMate (Matrix Technologies, Canada) and CNIS informer set drug library was added 24 hours later with a CyBio Well Vario (Analytik Jena AG, Germany). All 320 drugs were tested in duplicate using a series of 10-point dilutions ranging from 0.5nM to 10μM. Cell cultures were propagated and drug profiling performed at 37°C in a 5% CO2-humidified incubator. Cell viability was quantified 72 hours after drug treatment using CellTiter-Glo® luminescent assay. Raw luminescence signals were normalized to vehicle control for each drug. Drug curves were analyzed as outlined in methods above for CNIS. CNIS results on PDAC PDTOs are deposited in the CTD$^2$ Dataportal (https://ocg.cancer.gov/programs/ctd2/data-portal)).

### Preclinical PDAC Organoid Screening Platform

Patient data and tissue were obtained with written informed consent in accordance with the Declaration of Helsinki and were acquired through the Stanford University School of Medicine Institutional Review Board protocol #28908. Utilizing patient-derived pancreatic ductal adenocarcinoma tumor organoids (PDTOs: PDO 227, PDO 735, PDO 056) and a normal pancreas organoid (NPO-AS008N) from Stanford University, and (PDTOs: OPTR 3793, OPTR 7021) from the Brenden-Colson Center for Pancreatic Care, a preclinical PDAC organoid high-density platform was developed to generate high confidence dose response curves with novel agents and chemotherapeutics. Briefly, PDAC PDTOs and NPO were propagated in a modified Wnt-conditioned media in a 24 well culture plate format with Matrigel™ matrix at 37°C in a 5% CO2-humidified incubator based upon published methods for *in vitro* expansion of gastrointestinal stem cells and subsequent studies on patient-derived organoid culture (39,40) (20170523_OrganoidProtocols.pdf). PDAC PDTOs were passaged in a single cell format and combined with Matrigel™ matrix and arrayed in 96-well plate format at ~3 × $10^4$ patient derived cells in 6μl Matrigel/well and treated at 24hr with FDA-approved drugs for PDAC: gemcitabine, irinotecan, oxaliplatin, paclitaxel, everolimus, 5-fluorouracil, mitomycin c, and erlotinib (Selleckchem),

and novel investigative agents: Triptolide, Trametinib, SNS-032, THZ1, THZ531, AZD1775 (vendors listed above). Normal pancreas organoids (NPO) were allowed to establish for 168 hours after plating and prior to treatment protocol to model the *in vivo* condition. For all drugs, serial dilutions were performed to generate singleton 10-point dose response data with concentrations ranging from 1.5nM-50μM on all organoid models. Organoids were incubated at 37°C in 5% CO2 and cell viabilities were quantified 144 hours after drug treatment using CellTiterGlo 3D luminescent assay (Promega). Raw luminescence signals were normalized to vehicle control (v/v) for each drug. Drug curves were fitted and IC50s were calculated via non-linear regression utilizing a 3-parameter logistic dose response model in Prism version 9 (GraphPad Software Inc.).

### Statistical Analysis

All statistical analysis on RNAi screens is described under specific methods sections. Data between two groups were compared using a two-tailed unpaired t-test or the Mann–Whitney test as appropriate for the type of data (normality of distribution). Unless otherwise indicated, a P-value less than or equal to 0.05 was considered statistically significant for all analyses. Multiple groups were compared using the Kruskal-Wallis with Dunn's post-test or one-way ordinary ANOVA with Dunnett's post-test. All group results are represented as mean ± s.d., if not stated otherwise. Prism version 7–9 (GraphPad Software Inc.) was used for all these analyses.

### Data availability

The authors declare that all the data supporting the findings of this study are available within the article and the supporting information files, and from the corresponding authors upon reasonable request.

## Results

### Pancreatic cancer models for functional investigations

A surgical pancreatic tumor specimen was obtained during a pancreaticoduodenectomy performed on a 75-year-old female patient diagnosed with pancreatic adenocarcinoma (Histology - Grade 3). Information regarding subsequent treatment of this patient was not available, but the outcome of this treatment failed and the patient was deceased within a year. A patient-derived xenograft (PDX) of the tumor specimen was established in an immunodeficient NOD SCID gamma (NSG) mouse, and a low passage culture (referred to as PancVH1 PDCL or PancVH1) was subsequently established from this model. Genetic and pharmacological profiling was performed on this PancVH1 PDCL utilizing whole exome sequencing (WES), array CGH, a druggable genome RNAi screen, and comprehensive drug profiling (Fig.1A, Fig.S1A). Initial characterization performed on PancVH1 demonstrated KRAS activation (KRAS-GTP), increased downstream signaling via MEK phosphorylation, TP53 protein truncation, and decreased expression of CDKN2A ($p16^{Ink4a}$), and SMAD4 in comparison to HPNE cells (Fig.1B). The HPNE cell line was derived from the intermediary cells formed during acinar-to-ductal metaplasia (ADM) of the normal exocrine pancreas by transduction with a retroviral expression vector containing the catalytic subunit of human telomerase (hTERT). HPNE cells are diploid, fail to senesce,

are positive for telomerase, and express wildtype KRAS, TP53, CDKN2A ($p16^{Ink4a}$), and SMAD4, thus leaving intact cancer-associated somatic changes effecting key oncogenic and tumor suppressor pathways (36) (Fig.1B). The HPNE cell line is therefore a unique and tractable (i.e., immortalized but non-tumorigenic) pancreas epithelial cell line used extensively in this report to identify and prioritize potential therapeutic vulnerabilities in PDAC (Fig.S1A).

## Genomic characterization of PancVH1 identify alterations in *KRAS, TP53, CDKN2B, and SMAD3*

Whole-exome sequencing (WES) of PancVH1 identified 117 consensus coding sequence (CCDS) variants including genomic alterations in *KRAS G12V* effecting GTP hydrolysis, a truncating *TP53 R342** mutation compromising the p53 tetrameric complex, and a c-terminal MH2 domain loss in *SMAD3 C316** potentially disrupting the stability of the SMAD3/4 cofactor complex downstream of TGF-beta signaling. The *PTPN11 Y197** (Shp2) phosphatase was also identified as a potential driver gene via comparative analysis to cancer genome landscapes (41) (Fig.1C, Fig.S1B–C, SI Dataset 1A–F). Gene level comparative analysis of the 117 CCDS coding variants from PancVH1 to pancreatic cancer public genomic datasets (TCGA, ICGC, UTSW) show 14 genes in common with only 7 at a frequency >5% in at least one dataset including *KRAS, TP53, MUC4, RYR1, RYR2, CSMD1* and *MUC16* (CA125), a known cancer biomarker and neoantigen associated with long-term survival and with MHC/HLA reveal potential defects in antigen-processing and immune evasion (42) (Fig.S1D, SI Dataset S1A). In summary, this histological grade 3 PDAC patient has two signature genomic alterations in *KRAS* and *TP53,* and two genomic alterations which have the potential to phenocopy signature genomic alterations in SMAD4, with loss of interacting domain in SMAD3 cofactor complex, and CDKN2A, as array CGH results show a deep deletion in CDKN2B (p15Ink4b), a gene that lies adjacent to CDKN2A (p16Ink4a), and also encodes for a CDK4/6 inhibitor (SI Dataset S1G). This genomic signature of PancVH1 PDCL represents a poor prognosis, and as stated above this patient was deceased within a year (i.e., representative of a typical PDAC patient).

## Functional screening identifies CFLAR, the CDK-activating kinase (CAK) complex, and the CDK13 transcriptional kinase as potential targets in KRAS TP53 mutant PancVH1

Functional genomics is a powerful tool to discover cancer targets (26,27,43,44). High-throughput arrayed RNA interference (RNAi) phenotypic screening of a patient's cancer cells provides a complementary strategy to DNA sequencing for nominating potential driver mutations and identifying cancer-specific vulnerabilities. A druggable genome arrayed RNAi screen targeting 6659 genes was performed on PancVH1 cells (Fig.1D, Fig.S2A–C, SI Dataset S2A–F, $CTD^2$ Dataportal (https://ocg.cancer.gov/programs/ctd2/data-portal)). A custom pancreatic pathway control sublibrary targeting 50 genes was included to confirm the fidelity of the screen as well as to nominate high confidence druggable signaling nodes (Fig.1D). Screen results were integrated with PancVH1 somatic coding variants, PancVH1 CGH results, PDAC TCGA data (cBioportal), drug prioritization (i.e., availability of known drugs to targets), and RNAi screening results on KRAS mutant PDAC cell lines (JHU) to select 327 genes (5% - 327/6659) for subsequent testing (FDR <0.3) (Fig.1D, Fig.S2B–D, SI Dataset S2A–C). A custom RNAi secondary library was designed, constructed, and

arrayed utilizing independent siRNA pools (n=4) to these 327 selected gene targets with controls to KRAS, TP53, CDKN2A, and SMAD4, and a secondary screen was performed on PancVH1 and HPNE cells to confirm results from the primary screen and further prioritize PDAC specific targets (SI Dataset S3A–F). Forty-percent (132/331) of the selected gene targets in the secondary RNAi screen were validated in the secondary RNAi screen in PancVH1 cells (gene target siRNA pool vs. negative control siRNA); $-\log_{10}$ Pvalue >1 as significant (Fig.1E, SI Dataset S3A–B), a subset of which are currently druggable. Geneset overlap analysis of significant hits from the secondary screen with the molecular signatures database (MSigDB) was performed and revealed significant overlap of the KRAS_SHP2 (PTPN11) pathway including KRAS effectors RAF1 and RHOA (Fig.S3A), the MYC pathway including RRM1, apoptosis including CFLAR (CASP8 and FADD Like Apoptosis Regulator), cell cycle including CCNH (Cyclin H), WEE1, CHEK1, and CDK13, as well as the MAP kinase and TNF signaling pathways (FDR<0.05) (Fig.1E. SI Dataset S3C). Gene target rank differentials of the secondary RNAi screen results (inset) between PancVH1 and HPNE cells were calculated to identify and prioritize significant selective dependencies (i.e., preferential lethality, Pvalue <0.05) in the KRAS mutant PancVH1 cells. Gene target rank differentials between PancVH1 and HPNE cells were also cross referenced with mean rank differentials from RNAi extended kinome screens (1302 genes) on seven KRAS mutant PDAC cell lines (JHU) and HPNE cells (Fig.S2D, SI Dataset S3D), to further prioritize high confidence druggable signaling nodes including CDK13, CFLAR, and WEE1 (Fig.1F, Fig.S3B, SI Dataset S3E). As CCNH was a significant gene target hit and selectively dependent in PancVH1 cells we reasoned that CDK7, its corresponding kinase partner in the CDK activating complex (CAK), could also be a target and dependency. To address this, all three known protein partners of CAK: Cyclin H, CDK7, and MAT1 were independently immunoprecipitated from protein extracts, and immunoblotted to confirm CAK as a complex in PancVH1 and HPNE cells (Fig.S3C). CDK7 was subsequently shown to be a selectively dependent target in PancVH1 cells utilizing dicer-substrate siRNAs (dsiRNAs) (Fig.S3D). CFLAR was also further credentialed as a selectively dependent target (Fig.S3D).

## Drug profiling identifies the TFIIH complex as a potential target in KRAS mutant PDAC PDCLs

To identify active compounds and prioritize drug targets, we used dose-response assays to screen PancVH1 and HPNE cells with a 320-compound oncology-focused drug library known as the $CTD^2$ Network Informer set (CNIS). Active compounds with high potency in PancVH1 and with preferential activity compared to HPNE cells are shown (Fig.2A, SI Dataset S4A–E, $CTD^2$ DataPortal (https://ocg.cancer.gov/programs/ctd2/data-portal)). In parallel, low throughput drug profiling using dose-response assays were performed on PancVH1 and HPNE cells with 50 drugs/tool compounds curated from significant gene targets from the secondary RNAi screen, literature-based targets on PDAC biology, and epigenetic tool compounds from the Structural Genomics Consortium (SGC) (Fig.2B, SI Dataset S4F–G). This combination of unbiased and rational drug profiling of PancVH1 provided orthogonal evidence for gene targets identified from the druggable genome RNAi screen and also identified/confirmed known chemotherapeutics and targeted agents in preclinical/clinical development for PDAC, such as Gemcitabine (RRM1), YM155 (BIRC5),

AZD1775 (WEE1), Trametinib and PD0325901 (MEK1/MEK2), AZD7762 (CHEK1), CDDO-Me (MTOR), FK866 and GMX-1778 (NAMPT; NAD+ biosynthesis), OSI-906 and NVP-AEW541 (IGFR), Romidepsin (HDAC1/2), PIK-75 and BYL719 (PI3K), and JQ1(BRD2/3/4). In addition, Triptolide and SNS-032 were identified as potentially novel drugs for PDAC. These small molecules target XPB (45–47), and CDK7/CDK9 (48,49) respectively, which are part of the TFIIH complex, a ten-subunit complex involved in general transcription and DNA repair including the transcriptional and cell cycle CDK-activating kinase (CAK) subcomplex (50,51) (Fig.2B, SI Dataset S4).

From this comprehensive drug profiling, differential potencies observed between PancVH1 and HPNE cells, biochemical IC50/Ki(s) of specific compounds, and preclinical/clinical relevance to PDAC biology was utilized as criteria to select 22 known and novel targeted agents including a newly developed covalent CDK7/12/13 inhibitor, THZ1 (52) for further evaluation. Low throughput drug profiling was performed with these compounds, on a panel of 14 genomically (SV subtyped-Stable, Focal, Scattered, Unstable) and molecularly subtyped (classical pancreatic, squamous) PDCLs obtained from The Kinghorn Cancer Centre (TKCC) through the International Cancer Genome Consortium (ICGC) (Fig.2C, Fig.S4A–C). TKCC PDCLs were derived from tumor tissue isolated for genomic analysis in Waddell et al. 2015 (12), and genomic subtypes and molecular subtypes are further clarified in Chou et al. 2018 (28) and Dreyer et al. 2021 (53), respectively. TP53 CCDS coding variants in TKCC PDCLs were further clarified in this report (SI Dataset S5). Results from drug profiling TKCC PDCLs showed that while known compounds such as romidepsin, YM155, and bortezemib display broad cytotoxicity in the *in vitro* setting, and the MEK1/2, WEE1, and CHEK1 inhibitors display single-agent activity in KRAS mutant PDCLs as expected, potentially novel polypharmacological agents for PDAC, targeting the cyclin-dependent kinases (CDK), and specifically the transcriptional cyclin-dependent kinases, such as THZ1 (CDK7/12/13), SNS-032 (CDK7/9), and Triptolide (XPB/TFIIH) all show single-agent activity in KRAS mutant TKCC PDCLs (Fig.2C, SI Dataset S6A). Subsequent drug profiling was performed on an abridged panel of 11 KRAS mutant TKCC PDCLs for seven targeted agents using dose-response assays to validate the efficacy and potency of these agents. Sensitivity to all three TFIIH inhibitors [ THZ1 potency range: 41.7nM–1.1μM; median (145 nM); SNS-032 potency range:128–581nM; median (296 nM); Triptolide potency range: 1.4–24.5nM; median (7.3 nM)] was confirmed and all demonstrated broad single agent activity (<1μM) (Fig.2D). Sensitivity to all three TFIIH inhibitors was independent of the specific KRAS mutation (G12D, G12V, Q61H), TP53 mutational status, and genomic structural variant subtype (Stable, Scattered, and Unstable) (Fig.2D, SI Dataset S6B). The high potency and differential sensitivity of the TFIIH inhibitors between KRAS mutant PancVH1 PDCL and HPNE cells was again confirmed with fitted dose-response curves (Fig.2E). Together, this suggests a transcriptional dependency in KRAS mutant PDAC and a potential therapeutic vulnerability (i.e., therapeutic window) as all three compounds have an overlapping target.

## CFLAR, CDK7, and XPB were further credentialed as therapeutic targets in KRAS mutant PDAC PDCLs

CFLAR, CDK7, CCNH, XPB (ERCC3), CDK9 and CDK13 were subsequently investigated as potential targets utilizing dsiRNAs. PancVH1 was utilized initially to assess the efficacy of dsiRNAs in colony assays and protein target expression via immunoblots (Fig.S4D). DsiRNA pools to all six targets were next assessed on a panel of ten KRAS mutant TKCC PDCLs including PancVH1 with knockdown of CFLAR, CDK7, and XPB showing a significant effect on cellular viability in 10/10 cell lines, CCNH in 8/10, CDK9 in 4/10, and CDK13 in 3/10 cell lines (Fig.S4E).

## TFIIH inhibition initiates a CFLAR-mediated caspase-8 dependent apoptotic response in KRAS TP53 mutant PancVH1

Since CFLAR, a negative regulator of the extrinsic apoptotic pathway, scored as a top hit from our druggable genome RNAi screen (2/6659, Pvalue = $3.57 \times 10^{-4}$, qvalue = 0.014) (SI DataSet S2C), was validated as the top significant hit in the secondary RNAi screen (Pvalue = $8.306 \times 10^{-12}$) (Fig.1E, SI Dataset S3B), and was observed to be selectively dependent (i.e., preferentially lethal) in PancVH1 vs. HPNE cells (Pvalue = $7.664 \times 10^{-5}$) (Fig.1F, SI DataSet S3A, Fig.S3D), we asked whether the sensitivity to compounds targeting transcriptional cyclin-dependent kinases and the TFIIH complex, namely, CDK7/12/13 (THZ1), CDK7/9 (SNS-032), and Triptolide (XPB) (Fig.2), operated through a CFLAR-mediated mechanism of cell death. We found that treatment with these transcriptional CDK inhibitors, including THZ531, a CDK12/13 inhibitor (54), and TFIIH inhibitors reduced CFLAR expression in a concentration dependent manner in PancVH1 cells, with the TFIIH covalent inhibitors THZ1 and Triptolide showing the highest potencies (Fig.3A). Treatment of HPNE cells with these inhibitors did reduce CFLAR expression, but not in a concentration dependent manner. In corresponding immunoblots, we show that this concentration dependent reduction in CFLAR expression correlates with the induction of DNA damage and the activation of a caspase-8 apoptotic response (i.e., caspase-3 cleavage, PARP cleavage) in KRAS mutant PancVH1 cells. In contrast, no such apoptotic response was seen in HPNE cells, which instead upregulated p53-p21 with resolution of DNA damage, indicating cell cycle arrest and cellular survival (Fig.3B).

Cell cycle analysis further confirmed the apoptotic/antiproliferative effects of THZ1 on PancVH1 cells, which initiated a cell death response primarily at the G1/S transition with subsequent accumulation of sub-G1 DNA content (i.e., indicative of dead cells), while in HPNE cells, THZ1 treatment resulted in a G2 phase cell cycle arrest (Fig.S5A). Apoptotic and antiproliferative responses to THZ1 treatment were further confirmed via immunoblot in PancVH1 and HPNE cells (Fig.S5B). We also confirmed the known mechanism of action of THZ1 via dose dependent inhibition of phospho-substrates of CDK7, namely, $CDK2^{Thr160}$, $CDK1^{Thr161}$, and Serine 2 residues on the carboxy terminal domain (CTD) of RPB1 (also known as Pol II, RNA Pol II CTD, POLR2A), the largest subunit of RNA polymerase II, which is essential for the transcription of protein-coding genes (Fig.S5C). In addition, we confirmed that TFIIH inhibitors reduce CFLAR expression in a concentration and time-dependent manner with a concomitant increase in PARP cleavage in KRAS mutant PancVH1 PDCL (Fig.S5D, Fig.S6A). In contrast, CFLAR expression was not reduced

following treatment with AZD1775, a WEE1 kinase inhibitor with similar cytotoxicity in KRAS mutant PDCLs, suggesting a specific mechanism of action for transcriptional CDK/TFIIH inhibitors (Fig.S5D).

Using short-term cellular viability assays and caspase-8 specific inhibitors we demonstrate that compounds targeting the transcriptional cyclin-dependent kinases and the TFIIH complex, namely, CDK7/12/13 (THZ1), CDK7/9 (SNS-032), CDK12/13 (THZ531) and Triptolide (XPB) all induce cell death in a caspase-8 dependent manner in KRAS mutant PancVH1 PDCL, with no significant effect observed in HPNE cells (Fig.3C). In corresponding assays, all compounds induce caspase-8 activity in KRAS mutant PancVH1 PDCL, while having minimal effect on HPNE cells, all suggesting a shared mechanism of cell death through caspase-8 dependent apoptosis (Fig.3D). In both assays, and in agreement with immunoblotting results above, TFIIH inhibition directly, either with the CDK7/12/13 (THZ1), CDK7/9 (SNS-032), or Triptolide (XPB) inhibitor, as opposed to the transcriptional kinase CDK12/13 inhibitor (THZ531), have a more significant effect on CFLAR downregulation and caspase-8 activation. In sum, TFIIH inhibition initiates CFLAR-mediated caspase-8 dependent apoptosis in KRAS mutant PDCLs.

## TFIIH inhibition disrupts the protein stability of RPB1 resulting in the downregulation of IAPs and transcriptional effectors of oncogenic signaling in KRAS TP53 mutant PDAC PDCLs

Since TFIIH is an essential factor of RNA polymerase II transcription initiation (50,55), and transcriptional CDK inhibitors are under clinical investigation in multiple cancer types (56), we examined whether TFIIH inhibition could downregulate key protein regulators of cellular survival and transcriptional effectors that maintain an oncogenic phenotype in KRAS mutant PDAC. Here we show that TFIIH inhibition results in concentration-dependent downregulation of RPB1, CFLAR, and IAPs MCL1 and XIAP (Fig.4A). The TFIIH covalent inhibitors THZ1 and Triptolide showed the greatest effects on protein expression in all four KRAS TP53 mutant PDCLs tested. Gemcitabine, tested alongside these TFIIH inhibitors at concentrations that result in similar amount of DNA damage (H2A.X $^{Ser139}$), did not lead to a similar downregulation of these key protein regulators of cellular survival, demonstrating a distinction in the mechanism(s) of action of these inhibitors in both gemcitabine sensitive (top), and gemcitabine resistant (bottom) PDCLs (Fig.4A, Fig.2A–C). These results are also supported by time-dependent assays with THZ1, SNS-032, and Triptolide (Fig.S6A).

Since transcriptional effectors of KRAS mutant signaling such as STAT3, FOSL1 and MYC are involved in tumor maintenance and progression in PDAC (15,16,18–22) and inhibitors to TFIIH can clearly affect expression of RPB1 (Fig.4A), we reasoned that these transcriptional effectors could also be affected. Here we show that TFIIH inhibition results in a concentration dependent downregulation of STAT3 and FOSL1 transcription factors in four KRAS TP53 mutant PDCLs, with the covalent inhibitor Triptolide having the broadest and most potent effects in both gemcitabine sensitive (top) and resistant (bottom) PDCLs (Fig.4B, Fig.2A–C). These results are also supported by time-dependent assays with THZ1, SNS-032, and Triptolide and demonstrate some shared and distinct

time-dependent reductions in expression of STAT3, E2F1, FOSL1, FOSL2, and MYC in KRAS TP53 mutant PancVH1 PDCL (Fig.S6A). RPB1 expression was further examined via immunoblot upon treatment with THZ1, SNS-032, THZ531, and Triptolide in KRAS mutant PancVH1 and HPNE cells to demonstrate RPB1 transcriptional dependency was specific to KRAS mutant PDCL (Fig.S6B). To further elucidate the mechanism of action of these TFIIH inhibitors on RPB1 protein stability, we treated PancVH1 with THZ1, SNS-032, and Triptolide in combination with MG132, which inhibits the proteolytic activity of the 26S complex. Results show that RPB1 protein stability is in part regulated by the 26S complex upon treatment with THZ1, or SNS-032, but the effect of Triptolide on RPB1 protein stability appears to be mediated independently of the 26S proteasome complex (Fig.S6C).

TFIIH is an essential factor for RNA polymerase II transcription initiation, and these results support a model whereby inhibition of TFIIH, including the CAK subcomplex with THZ1, SNS-032, and Triptolide disrupts the protein stability and coordinated phosphorylation of Serine2, Serine5, Serine7 residues of the 52 heptapeptide repeat (Y1S2P3T4S5P6S7) carboxy-terminal domain (CTD) of RPB1, thereby disrupting the spatiotemporal code (57) that instructs ordered engagement of RNA polymerase II transcription. CDK7 also phosphorylates the activating T-loop of the CDK9 transcriptional kinase component of the positive transcriptional elongation factor (P-TEFb), which in turn phosphorylates RPB1 CTD required for transcriptional elongation (58), so inhibition of the TFIIH complex could also regulate CDK9 activity and transcriptional elongation. The transcriptional kinase CDK13 also phosphorylates RPB1/RNA Pol II CTD and is involved primarily in regulating pre-mRNA splicing in RNA polymerase II transcription (59) (Fig.4C). In summary, TFIIH and transcriptional CDK inhibitors disrupt the largest subunit of RNA polymerase II, RNA polymerase II Subunit B1 resulting in the downregulation of IAPs and transcriptional effectors of KRAS mutant signaling in PDAC.

## TFIIH inhibition in combination with TRAIL as a potential therapeutic strategy for PDAC

Since CFLAR, a negative regulator of the death receptor induced signaling complex, was identified as a top druggable signaling node and potential therapeutic target, and TFIIH inhibitors transcriptionally downregulate CFLAR, and key IAPs, namely, MCL1 and XIAP that regulate critical steps in the execution of mitochondrial-mediated apoptosis, we reasoned that a combination treatment with TRAIL (TNF-related apoptosis inducing ligand), which selectively kills cancer cells via death-receptor-mediated apoptosis (60,61), could cooperate with TFIIH inhibitors to optimize and amplify a programmed cell death response in pancreatic ductal adenocarcinoma (Fig.5A).

One of the hallmarks of cancer is evading apoptosis, and in pancreatic ductal adenocarcinoma, frequent mutations in the p53 gene likely disable the intrinsic mitochondrial-mediated apoptotic pathway (62). Using genomic and copy number variation data compiled in cBioPortal public datasets (QCMG, UTSW, ICGC) on pancreatic adenocarcinoma patients, we confirm the high frequency of p53 mutation, and the low incidence (≤ 0.5% for all 17 genes examined) of somatic mutations (591 patients) and deep deletions (i.e., copy number variations, 293 patients) in genes involved in the extrinsic apoptosis pathway (Fig.5B). Therefore, the fidelity of the extrinsic apoptotic pathway likely

remains intact in PDAC patients and the response to treatment with TRAIL, and the modulation of key apoptotic regulators through TFIIH inhibition, may not be compromised by somatic alterations. Even so, *TNFRSF10A* and *TNFRSF10B,* genes coding for the TRAIL-R1 (DR4), and TRAIL-R2 (DR5) receptors respectively, show a 2.0% incidence of deep deletion in this dataset, and represent a distinct subset in which this combination therapy in patients could be contraindicated (Fig.5B). All PDCLs used in this study were examined for somatic mutations in 17 extrinsic apoptotic pathway genes with only one of these, TKCC-05, harboring a reported missense mutation in one gene, *BIRC5* (Fig.S7A, SI Dataset S1). Protein expression of both TRAIL-R1 (DR4) and TRAIL-R2 (DR5) receptors were confirmed via immunoblot in all PDCLs and HPNE cells utilized in these investigations (Fig.S7B).

As TRAIL has been shown to selectively induce apoptosis in tumor cells (60,61), we performed dose response assays with TRAIL on HPNE, KRAS mutant PancVH1 PDCL, and ten KRAS mutant TKCC PDCLs to show that indeed, TRAIL (izTRAIL) selectively kills KRAS mutant PDCLs compared to HPNE cells (Fig.5C). BID (BH3 interacting domain death agonist) cleavage, the target of caspase-8 activity that is induced upon treatment with TRAIL, is a critical event that generates tBid which in turn oligomerizes with pro-apoptotic Bak/Bax family members at the outer mitochondrial membrane to facilitate the release of cytochrome c (i.e., apoptosome formation), during death receptor-mediated apoptosis (63–65) (Fig.5A). Here we show that treatment of KRAS mutant PancVH1 with TRAIL at 25 ng/ml (~EC50 concentration) engages death receptor mediated apoptosis but does not cleave BID, and as expected, no such effect is seen in TRAIL treated HPNE cells (Fig.5D). However, in combination with TFIIH inhibitors THZ1, SNS-032, and Triptolide, TRAIL treatment results in the complete cleavage of BID with a concomitant increase in apoptosis as measured by PARP cleavage in PancVH1 (Fig.5D). As expected, and as a control for mechanism of action, TRAIL treatment in combination with gemcitabine, does result in increased cell death, but no BID cleavage is observed (Fig.5D). We further show the broader efficacy of this combination treatment with TRAIL and Triptolide, resulting in BID cleavage and an amplified apoptotic response in three additional KRAS mutant PDCLs, while no equivalent response was observed in HPNE cells (Fig.5E).

These results suggest that TRAIL and TFIIH inhibitors would exhibit a synergistic effect if used in combination in KRAS mutant pancreatic cancer. To test this hypothesis, we treated a panel of eleven KRAS mutant PDCLs with a 36-point dose response matrix (6 × 6 - TRAIL × TFIIH inhibitors). We examined the synergy between TRAIL and TFIIH inhibitors (THZ1, SNS-032, Triptolide) by computing the excess growth inhibition over the Bliss independence model (38), for each combination of TRAIL and TFIIH inhibitor concentrations. A synergy score (Bliss Sum) was computed for each combination experiment in each of the 11 KRAS mutant PDCLs by summing the excess over Bliss independence across all combinations. Indeed, TRAIL and TFIIH inhibitors exhibit a synergistic effect in combination in 10/11 KRAS mutant PDCLs examined (Fig.5F).

### Preclinical Pancreatic Cancer Patient-derived Tumor Organoid Models

Here we also demonstrate the utility of pancreatic cancer patient-derived tumor organoids (PDTOs) in a high throughput screening format with the CTD$^2$ Network Informer Set (CNIS) drug library and confirm the efficacy of Triptolide in KRAS mutant PDAC organoid models (Fig.S8A–B, CTD$^2$ DataPortal (https://ocg.cancer.gov/programs/ctd2/data-portal)). We also demonstrate the utility of a novel preclinical organoid screening platform on five KRAS mutant PDAC PDTO models and a normal pancreas organoid (NPO) model to validate the efficacy of these TFIIH/XPB/transcriptional cyclin-dependent kinase inhibitors alongside FDA approved agents for pancreatic cancer (Fig.S8C–D).

## Discussion

In this report, we utilized a functional approach integrating genomic, functional genetic, and pharmacological profiling on a patient-derived tumor cell culture with signature genomic alterations indicative of a metastatic phenotype and poor prognosis, to nominate key druggable signaling nodes and potential therapeutic targets for pancreatic ductal adenocarcinoma. This functional genetic approach identified CFLAR, the CAK complex, and the CDK13 transcriptional kinase as potential vulnerabilities in KRAS mutant PDAC. These results are consistent with CFLAR as a critical regulator of apoptosis in pancreatic cancer cells (66), and a transcriptional dependency in cancer (56). Drug profiling confirmed the efficacy of known targets and drugs for PDAC and revealed a therapeutic vulnerability and dependence on the general transcription and DNA repair factor TFIIH, particularly the XPB subunit and CAK ternary complex, essential for RNA polymerase II transcription. TFIIH inhibition with a covalent inhibitor of CDK7/12/13, THZ1, a CDK7/CDK9 kinase inhibitor, SNS-032, a covalent inhibitor of XPB, Triptolide, all displayed broad single agent activity, and in the case of Triptolide, high potency in KRAS mutant PDCLs, presumably owing to its additional role in nucleotide excision repair (67,68).

We show that TFIIH inhibition broadly effects RNA polymerase II transcription by disrupting protein stability and signaling to RPB1 to downregulate key protein regulators of cellular survival, namely CFLAR, IAPs (MCL1, XIAP), and transcriptional effectors (STAT3, FOSL1) that maintain an oncogenic phenotype in KRAS mutant PDAC, with the covalent inhibitors THZ1 and Triptolide showing the most profound effects. As transcriptional effectors of KRAS mutant signaling are involved in tumor maintenance and progression in PDAC, and current investigations (69) are focused on identifying and targeting transcriptional programs to remodel stroma, extracellular matrix, inflammatory signaling, and an immune suppressive microenvironment in PDAC, these results could have direct translational potential in support of these efforts.

Since TFIIH inhibition could concomitantly downregulate CFLAR, the negative regulator of death receptor-mediated apoptosis, and critical inhibitors of mitochondrial-mediated apoptosis, namely, MCL1, and XIAP, we hypothesized that a combination therapy with TRAIL and TFIIH inhibitors could amplify a programmed cell death response in KRAS mutant PDAC. Indeed, this is the case, as TRAIL and TFIIH inhibitors exhibit a synergistic effect in combination in KRAS mutant PDCLs. It should be noted, that all results reported here utilized izTRAIL (stable trimer-AdipoGen), a highly active recombinant form of

soluble human TRAIL designed with a trimerizing N-terminal isoleucine zipper motif that induces apoptosis in human cancer cells *in vitro,* with no observed activity in primary human hepatocytes. Consistent with our results, a recently developed hexavalent TRAIL agonist (ABBV-621) has demonstrated combination efficacy with a metabolite of irinotecan, SN-38, an inhibitor of DNA topoisomerase I with an important role in transcription, and a selective inhibitor of BCl-$X_L$ in preclinical pancreatic PDX models (70), and is currently in Phase I trials in chemotherapy combination cohorts for metastatic KRAS mutant colorectal and pancreatic cancer patients (NCT03082209). These results and others are consistent with a model of TRAIL-induced apoptosis in which multimeric variants of a TRAIL agonist, in combination with TFIIH/transcriptional CDK inhibitors as potent sensitizers, can optimize a programmed cell death response, even in the context of KRAS TP53 mutations (71, 72).

Preclinical investigations have previously demonstrated the efficacy of Triptolide (Minnelide) in multiple preclinical pancreatic cancer models (73). Our results utilizing novel patient-derived xenograft tumor cell culture (PDCL) models and patient-derived tumor organoid (PDTO) models are consistent with these investigations, and demonstrate the utility of these novel preclinical models for validating and prioritizing novel therapeutic agents for pancreatic cancer patients.

Clinically, Phase I trial results with Minnelide have shown promising activity in patients (74), and currently, a Phase II International open label clinical trial of Minnelide in patients with chemotherapy refractory metastatic pancreatic cancer (MinPAC) (NCT03117920) is in progress (75), results of which are highly anticipated by the pancreatic cancer community. Our results suggest a novel combination therapy in which systemic and acute treatment with the hexavalent TRAIL agonist (ABBV-621), in the context of the TFIIH inhibitor Triptolide or transcriptional CDK inhibitors could have direct translational implications on current clinical trials in PDAC patients.

## Supplementary Material

Refer to Web version on PubMed Central for supplementary material.

## ACKNOWLEDGMENTS.

We would like to thank members of the Kemp, Mendez, Biankin, and Von Hoff laboratories for helpful discussions. This work was supported by grants U01CA217883, R01CA21428, Canary Foundation, Listwin Foundation, and Gregory Fund to C.K., National Foundation for Cancer Research, The Seena Magovitz Foundation, Lee T. Hanley Fund for Pancreatic Cancer Research, and StandUpToCancer to H.H. and D.V.H. We would especially like to thank Daniela Gerhard, the Program Director of the NCI Office of Cancer Genomics and the $CTD^2$ Cancer Target Discovery and Development Program for her support of this research.

## References

1. Siegel RL, Miller KD, Jemal A. Cancer statistics, 2018. CA Cancer J Clin 2018;68:7–30 [PubMed: 29313949]
2. Sohn TA, Yeo CJ, Cameron JL, Koniaris L, Kaushal S, Abrams RA, et al. Resected adenocarcinoma of the pancreas-616 patients: results, outcomes, and prognostic indicators. J Gastrointest Surg 2000;4:567–79 [PubMed: 11307091]

3. Burris HA 3rd, Moore MJ, Andersen J, Green MR, Rothenberg ML, Modiano MR, et al. Improvements in survival and clinical benefit with gemcitabine as first-line therapy for patients with advanced pancreas cancer: a randomized trial. J Clin Oncol 1997;15:2403–13 [PubMed: 9196156]
4. Conroy T, Desseigne F, Ychou M, Bouche O, Guimbaud R, Becouarn Y, et al. FOLFIRINOX versus gemcitabine for metastatic pancreatic cancer. N Engl J Med 2011;364:1817–25 [PubMed: 21561347]
5. Von Hoff DD, Ervin T, Arena FP, Chiorean EG, Infante J, Moore M, et al. Increased survival in pancreatic cancer with nab-paclitaxel plus gemcitabine. N Engl J Med 2013;369:1691–703 [PubMed: 24131140]
6. Enzler T, Bates S. Clinical Trials in Pancreatic Cancer: A Long Slog. Oncologist 2017;22:1424–6 [PubMed: 28982802]
7. Yu J, Blackford AL, Dal Molin M, Wolfgang CL, Goggins M. Time to progression of pancreatic ductal adenocarcinoma from low-to-high tumour stages. Gut 2015;64:1783–9 [PubMed: 25636698]
8. Yachida S, White CM, Naito Y, Zhong Y, Brosnan JA, Macgregor-Das AM, et al. Clinical significance of the genetic landscape of pancreatic cancer and implications for identification of potential long-term survivors. Clin Cancer Res 2012;18:6339–47 [PubMed: 22991414]
9. Makohon-Moore AP, Zhang M, Reiter JG, Bozic I, Allen B, Kundu D, et al. Limited heterogeneity of known driver gene mutations among the metastases of individual patients with pancreatic cancer. Nat Genet 2017;49:358–66 [PubMed: 28092682]
10. Zehir A, Benayed R, Shah RH, Syed A, Middha S, Kim HR, et al. Mutational landscape of metastatic cancer revealed from prospective clinical sequencing of 10,000 patients. Nat Med 2017;23:703–13 [PubMed: 28481359]
11. Kleeff J, Korc M, Apte M, La Vecchia C, Johnson CD, Biankin AV, et al. Pancreatic cancer. Nat Rev Dis Primers 2016;2:16022 [PubMed: 27158978]
12. Waddell N, Pajic M, Patch AM, Chang DK, Kassahn KS, Bailey P, et al. Whole genomes redefine the mutational landscape of pancreatic cancer. Nature 2015;518:495–501 [PubMed: 25719666]
13. Bailey P, Chang DK, Nones K, Johns AL, Patch AM, Gingras MC, et al. Genomic analyses identify molecular subtypes of pancreatic cancer. Nature 2016;531:47–52 [PubMed: 26909576]
14. Dreyer SB, Chang DK, Bailey P, Biankin AV. Pancreatic Cancer Genomes: Implications for Clinical Management and Therapeutic Development. Clin Cancer Res 2017;23:1638–46 [PubMed: 28373362]
15. Laklai H, Miroshnikova YA, Pickup MW, Collisson EA, Kim GE, Barrett AS, et al. Genotype tunes pancreatic ductal adenocarcinoma tissue tension to induce matricellular fibrosis and tumor progression. Nat Med 2016;22:497–505 [PubMed: 27089513]
16. Nagathihalli NS, Castellanos JA, Shi C, Beesetty Y, Reyzer ML, Caprioli R, et al. Signal Transducer and Activator of Transcription 3, Mediated Remodeling of the Tumor Microenvironment Results in Enhanced Tumor Drug Delivery in a Mouse Model of Pancreatic Cancer. Gastroenterology 2015;149:1932–43 e9 [PubMed: 26255562]
17. Wormann SM, Song L, Ai J, Diakopoulos KN, Kurkowski MU, Gorgulu K, et al. Loss of P53 Function Activates JAK2-STAT3 Signaling to Promote Pancreatic Tumor Growth, Stroma Modification, and Gemcitabine Resistance in Mice and Is Associated With Patient Survival. Gastroenterology 2016;151:180–93 e12 [PubMed: 27003603]
18. Vallejo A, Perurena N, Guruceaga E, Mazur PK, Martinez-Canarias S, Zandueta C, et al. An integrative approach unveils FOSL1 as an oncogene vulnerability in KRAS-driven lung and pancreatic cancer. Nat Commun 2017;8:14294 [PubMed: 28220783]
19. Hayashi A, Fan J, Chen R, Ho Y-j, Makohon-Moore AP, Lecomte N, et al. A unifying paradigm for transcriptional heterogeneity and squamous features in pancreatic ductal adenocarcinoma. Nature Cancer 2020;1:59–74 [PubMed: 35118421]
20. Collins MA, Bednar F, Zhang Y, Brisset JC, Galban S, Galban CJ, et al. Oncogenic Kras is required for both the initiation and maintenance of pancreatic cancer in mice. J Clin Invest 2012;122:639–53 [PubMed: 22232209]
21. Sodir NM, Kortlever RM, Barthet VJA, Campos T, Pellegrinet L, Kupczak S, et al. MYC Instructs and Maintains Pancreatic Adenocarcinoma Phenotype. Cancer Discov 2020;10:588–607 [PubMed: 31941709]

22. Li Y, He Y, Peng J, Su Z, Li Z, Zhang B, et al. Mutant Kras co-opts a proto-oncogenic enhancer network in inflammation-induced metaplastic progenitor cells to initiate pancreatic cancer. Nature Cancer 2021;2:49–65 [PubMed: 35121887]
23. Pishvaian MJ, Blais EM, Brody JR, Lyons E, DeArbeloa P, Hendifar A, et al. Overall survival in patients with pancreatic cancer receiving matched therapies following molecular profiling: a retrospective analysis of the Know Your Tumor registry trial. Lancet Oncol 2020;21:508–18 [PubMed: 32135080]
24. Cuneo KC, Morgan MA, Sahai V, Schipper MJ, Parsels LA, Parsels JD, et al. Dose Escalation Trial of the Wee1 Inhibitor Adavosertib (AZD1775) in Combination With Gemcitabine and Radiation for Patients With Locally Advanced Pancreatic Cancer. Journal of Clinical Oncology 2019;37:2643–50 [PubMed: 31398082]
25. Golan T, Hammel P, Reni M, Van Cutsem E, Macarulla T, Hall MJ, et al. Maintenance Olaparib for Germline BRCA-Mutated Metastatic Pancreatic Cancer. N Engl J Med 2019;381:317–27 [PubMed: 31157963]
26. Moser R, Xu C, Kao M, Annis J, Lerma LA, Schaupp CM, et al. Functional kinomics identifies candidate therapeutic targets in head and neck cancer. Clin Cancer Res 2014;20:4274–88 [PubMed: 25125259]
27. Xu C, Nikolova O, Basom RS, Mitchell RM, Shaw R, Moser RD, et al. Functional Precision Medicine Identifies Novel Druggable Targets and Therapeutic Options in Head and Neck Cancer. Clin Cancer Res 2018;24:2828–43 [PubMed: 29599409]
28. Chou A, Froio D, Nagrial AM, Parkin A, Murphy KJ, Chin VT, et al. Tailored first-line and second-line CDK4-targeting treatment combinations in mouse models of pancreatic cancer. Gut 2018;67:2142–55 [PubMed: 29080858]
29. Koboldt DC, Zhang Q, Larson DE, Shen D, McLellan MD, Lin L, et al. VarScan 2: somatic mutation and copy number alteration discovery in cancer by exome sequencing. Genome Res 2012;22:568–76 [PubMed: 22300766]
30. Cibulskis K, Lawrence MS, Carter SL, Sivachenko A, Jaffe D, Sougnez C, et al. Sensitive detection of somatic point mutations in impure and heterogeneous cancer samples. Nat Biotechnol 2013;31:213–9 [PubMed: 23396013]
31. Barrett MT, Deiotte R, Lenkiewicz E, Malasi S, Holley T, Evers L, et al. Clinical study of genomic drivers in pancreatic ductal adenocarcinoma. Br J Cancer 2017;117:572–82 [PubMed: 28720843]
32. Birmingham A, Selfors LM, Forster T, Wrobel D, Kennedy CJ, Shanks E, et al. Statistical methods for analysis of high-throughput RNA interference screens. Nat Methods 2009;6:569–75 [PubMed: 19644458]
33. Chung N, Zhang XD, Kreamer A, Locco L, Kuan PF, Bartz S, et al. Median absolute deviation to improve hit selection for genome-scale RNAi screens. J Biomol Screen 2008;13:149–58 [PubMed: 18216396]
34. Harsha HC, Kandasamy K, Ranganathan P, Rani S, Ramabadran S, Gollapudi S, et al. A compendium of potential biomarkers of pancreatic cancer. PLoS Med 2009;6:e1000046 [PubMed: 19360088]
35. Jaffee EM, Schutte M, Gossett J, Morsberger LA, Adler AJ, Thomas M, et al. Development and characterization of a cytokine-secreting pancreatic adenocarcinoma vaccine from primary tumors for use in clinical trials. Cancer J Sci Am 1998;4:194–203 [PubMed: 9612602]
36. Lee KM, Nguyen C, Ulrich AB, Pour PM, Ouellette MM. Immortalization with telomerase of the Nestin-positive cells of the human pancreas. Biochem Biophys Res Commun 2003;301:1038–44 [PubMed: 12589817]
37. Subramanian A, Tamayo P, Mootha VK, Mukherjee S, Ebert BL, Gillette MA, et al. Gene set enrichment analysis: a knowledge-based approach for interpreting genome-wide expression profiles. Proc Natl Acad Sci U S A 2005;102:15545–50 [PubMed: 16199517]
38. Bliss CI. The toxicity of poisons applied jointly. Annals of Applied Biology 1939;26:585–615
39. Miyoshi H, Stappenbeck TS. In vitro expansion and genetic modification of gastrointestinal stem cells in spheroid culture. Nat Protoc 2013;8:2471–82 [PubMed: 24232249]
40. Boj SF, Hwang CI, Baker LA, Chio II, Engle DD, Corbo V, et al. Organoid models of human and mouse ductal pancreatic cancer. Cell 2015;160:324–38 [PubMed: 25557080]

41. Vogelstein B, Papadopoulos N, Velculescu VE, Zhou S, Diaz LA Jr., Kinzler KW. Cancer genome landscapes. Science 2013;339:1546–58 [PubMed: 23539594]
42. Balachandran VP, Luksza M, Zhao JN, Makarov V, Moral JA, Remark R, et al. Identification of unique neoantigen qualities in long-term survivors of pancreatic cancer. Nature 2017;551:512–6 [PubMed: 29132146]
43. Mullenders J, Bernards R. Loss-of-function genetic screens as a tool to improve the diagnosis and treatment of cancer. Oncogene 2009;28:4409–20 [PubMed: 19767776]
44. Toyoshima M, Howie HL, Imakura M, Walsh RM, Annis JE, Chang AN, et al. Functional genomics identifies therapeutic targets for MYC-driven cancer. Proc Natl Acad Sci U S A 2012;109:9545–50 [PubMed: 22623531]
45. Kupchan SM, Court WA, Dailey RG Jr., Gilmore CJ, Bryan RF. Triptolide and tripdiolide, novel antileukemic diterpenoid triepoxides from Tripterygium wilfordii. J Am Chem Soc 1972;94:7194–5 [PubMed: 5072337]
46. Titov DV, Gilman B, He QL, Bhat S, Low WK, Dang Y, et al. XPB, a subunit of TFIIH, is a target of the natural product triptolide. Nat Chem Biol 2011;7:182–8 [PubMed: 21278739]
47. He QL, Titov DV, Li J, Tan M, Ye Z, Zhao Y, et al. Covalent modification of a cysteine residue in the XPB subunit of the general transcription factor TFIIH through single epoxide cleavage of the transcription inhibitor triptolide. Angew Chem Int Ed Engl 2015;54:1859–63 [PubMed: 25504624]
48. Misra RN, Xiao HY, Kim KS, Lu S, Han WC, Barbosa SA, et al. N-(cycloalkylamino)acyl-2-aminothiazole inhibitors of cyclin-dependent kinase 2. N-[5-[[[5-(1,1-dimethylethyl)-2-oxazolyl]methyl]thio]-2-thiazolyl]-4- piperidinecarboxamide (BMS-387032), a highly efficacious and selective antitumor agent. J Med Chem 2004;47:1719–28 [PubMed: 15027863]
49. Chen R, Wierda WG, Chubb S, Hawtin RE, Fox JA, Keating MJ, et al. Mechanism of action of SNS-032, a novel cyclin-dependent kinase inhibitor, in chronic lymphocytic leukemia. Blood 2009;113:4637–45 [PubMed: 19234140]
50. Compe E, Egly JM. TFIIH: when transcription met DNA repair. Nat Rev Mol Cell Biol 2012;13:343–54 [PubMed: 22572993]
51. Fisher RP. Secrets of a double agent: CDK7 in cell-cycle control and transcription. J Cell Sci 2005;118:5171–80 [PubMed: 16280550]
52. Kwiatkowski N, Zhang T, Rahl PB, Abraham BJ, Reddy J, Ficarro SB, et al. Targeting transcription regulation in cancer with a covalent CDK7 inhibitor. Nature 2014;511:616–20 [PubMed: 25043025]
53. Dreyer SB, Upstill-Goddard R, Paulus-Hock V, Paris C, Lampraki EM, Dray E, et al. Targeting DNA Damage Response and Replication Stress in Pancreatic Cancer. Gastroenterology 2021;160:362–77 e13 [PubMed: 33039466]
54. Zhang T, Kwiatkowski N, Olson CM, Dixon-Clarke SE, Abraham BJ, Greifenberg AK, et al. Covalent targeting of remote cysteine residues to develop CDK12 and CDK13 inhibitors. Nat Chem Biol 2016;12:876–84 [PubMed: 27571479]
55. Bywater MJ, Pearson RB, McArthur GA, Hannan RD. Dysregulation of the basal RNA polymerase transcription apparatus in cancer. Nat Rev Cancer 2013;13:299–314 [PubMed: 23612459]
56. Bradner JE, Hnisz D, Young RA. Transcriptional Addiction in Cancer. Cell 2017;168:629–43 [PubMed: 28187285]
57. Eick D, Geyer M. The RNA Polymerase II Carboxy-Terminal Domain (CTD) Code. Chemical Reviews 2013;113:8456–90 [PubMed: 23952966]
58. Larochelle S, Amat R, Glover-Cutter K, Sanso M, Zhang C, Allen JJ, et al. Cyclin-dependent kinase control of the initiation-to-elongation switch of RNA polymerase II. Nat Struct Mol Biol 2012;19:1108–15 [PubMed: 23064645]
59. Greifenberg AK, Honig D, Pilarova K, Duster R, Bartholomeeusen K, Bosken CA, et al. Structural and Functional Analysis of the Cdk13/Cyclin K Complex. Cell Rep 2016;14:320–31 [PubMed: 26748711]
60. Walczak H, Miller RE, Ariail K, Gliniak B, Griffith TS, Kubin M, et al. Tumoricidal activity of tumor necrosis factor-related apoptosis-inducing ligand in vivo. Nat Med 1999;5:157–63 [PubMed: 9930862]

61. Ashkenazi A, Pai RC, Fong S, Leung S, Lawrence DA, Marsters SA, et al. Safety and antitumor activity of recombinant soluble Apo2 ligand. J Clin Invest 1999;104:155–62 [PubMed: 10411544]
62. Mihara M, Erster S, Zaika A, Petrenko O, Chittenden T, Pancoska P, et al. p53 has a direct apoptogenic role at the mitochondria. Mol Cell 2003;11:577–90 [PubMed: 12667443]
63. Wei MC, Lindsten T, Mootha VK, Weiler S, Gross A, Ashiya M, et al. tBID, a membrane-targeted death ligand, oligomerizes BAK to release cytochrome c. Genes Dev 2000;14:2060–71 [PubMed: 10950869]
64. Schug ZT, Gonzalvez F, Houtkooper RH, Vaz FM, Gottlieb E. BID is cleaved by caspase-8 within a native complex on the mitochondrial membrane. Cell Death Differ 2011;18:538–48 [PubMed: 21072056]
65. Huang K, Zhang J, O'Neill KL, Gurumurthy CB, Quadros RM, Tu Y, et al. Cleavage by Caspase 8 and Mitochondrial Membrane Association Activate the BH3-only Protein Bid during TRAIL-induced Apoptosis. J Biol Chem 2016;291:11843–51 [PubMed: 27053107]
66. Haag C, Stadel D, Zhou S, Bachem MG, Moller P, Debatin KM, et al. Identification of c-FLIP(L) and c-FLIP(S) as critical regulators of death receptor-induced apoptosis in pancreatic cancer cells. Gut 2011;60:225–37 [PubMed: 20876774]
67. Compe E, Egly JM. Nucleotide Excision Repair and Transcriptional Regulation: TFIIH and Beyond. Annu Rev Biochem 2016;85:265–90 [PubMed: 27294439]
68. Greber BJ, Toso DB, Fang J, Nogales E. The complete structure of the human TFIIH core complex. Elife 2019;8
69. Evan GI, Hah N, Littlewood TD, Sodir NM, Campos T, Downes M, et al. Re-engineering the Pancreas Tumor Microenvironment: A "Regenerative Program" Hacked. Clin Cancer Res 2017;23:1647–55 [PubMed: 28373363]
70. Phillips DC, Buchanan FG, Cheng D, Solomon LR, Xiao Y, Xue J, et al. Hexavalent TRAIL Fusion Protein Eftozanermin Alfa Optimally Clusters Apoptosis-Inducing TRAIL Receptors to Induce On-Target Antitumor Activity in Solid Tumors. Cancer Res 2021;81:3402–14 [PubMed: 33687950]
71. von Karstedt S, Montinaro A, Walczak H. Exploring the TRAILs less travelled: TRAIL in cancer biology and therapy. Nat Rev Cancer 2017;17:352–66 [PubMed: 28536452]
72. Lemke J, von Karstedt S, Abd El Hay M, Conti A, Arce F, Montinaro A, et al. Selective CDK9 inhibition overcomes TRAIL resistance by concomitant suppression of cFlip and Mcl-1. Cell Death Differ 2014;21:491–502 [PubMed: 24362439]
73. Chugh R, Sangwan V, Patil SP, Dudeja V, Dawra RK, Banerjee S, et al. A preclinical evaluation of Minnelide as a therapeutic agent against pancreatic cancer. Sci Transl Med 2012;4:156ra39
74. Greeno E, Borazanci E, Gockerman J, Korn R, Saluja A, Von Hoff D. Abstract CT207: Phase I dose escalation and pharmokinetic study of 14-O-phosphonooxymethyltriptolide. Cancer Research 2015;75:CT207
75. Propper D, Han H, Hoff DV, Borazanci E, Reya T, Ghergurovich J, et al. Abstract CT165: Phase II open label trial of minnelide™ in patients with chemotherapy refractory metastatic pancreatic cancer. Cancer Research 2019;79:CT165

## Significance Statement

This study utilizes functional genetic and pharmacological profiling of KRAS mutant pancreatic adenocarcinoma to identify therapeutic strategies and finds that TFIIH inhibition synergizes with TRAIL to induce apoptosis in KRAS-driven pancreatic cancer.

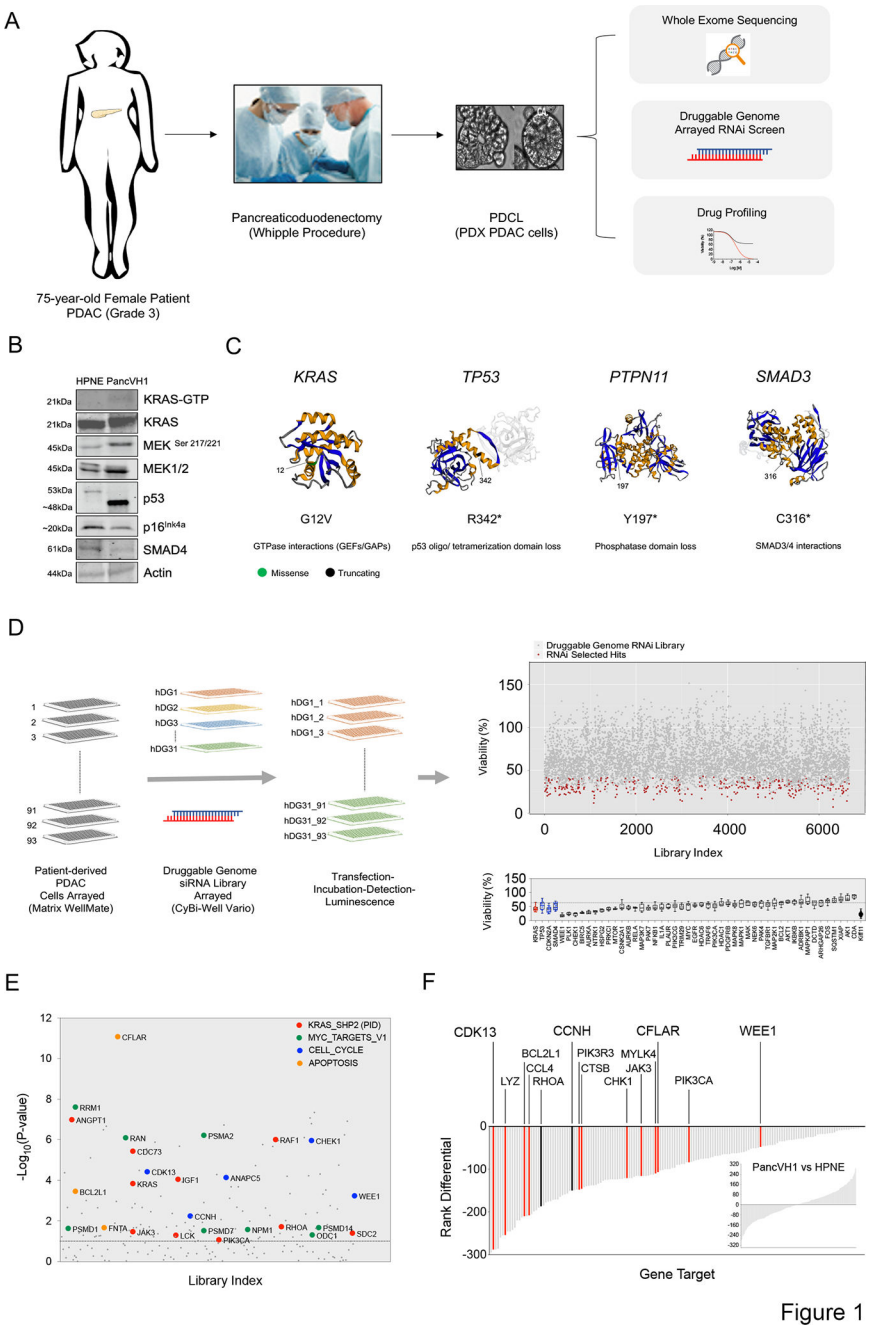


Figure 1

**Figure 1. Molecular and functional profiling identifies CFLAR, the CAK complex, and the transcriptional kinase CDK13 as potential therapeutic targets in KRAS TP53 mutant PancVH1 PDCL.**

**A**. Schematic overview of molecular and functional profiling of PancVH1 cells. **B**. PancVH1 immunoblot characterization of KRAS signaling - KRAS-GTP, MEK activation (MEK Ser217/221), truncation of the p53 protein, and reduction in expression of CDNK2A (p16Ink4a), and SMAD4 (DPC4). HPNE cell line used as a non-tumorigenic control. **C**. PancVH1 candidate driver genes as defined by cross reference to cancer landscapes. **D**. Left panel: schematic of druggable genome RNAi arrayed screen; 93 cell seeded plates;

31 siRNA library plates (hDG1-hDG31) with transfection reagents arrayed in triplicate on 93 cell seeded plates. Right panel: PancVH1 Druggable Genome RNAi screen results as mean (n=3) percent viability (y -axis) and library index of 6659 targeted genes (x-axis) with 327 (5%) RNAi selected hits (red). Lower panel; pancreatic pathway siRNA controls sublibrary to KRAS (n=108), TP53 (n=93), CDKN2A (n=93), SMAD4 (n=93) and 46 genes (n=18–21) compiled from the literature, KIF11 positive control (n= 744). **E**. PancVH1 RNAi secondary screen significant hits ($-\log_{10}$P-value > 1; dotted line denotes - $\log_{10}$P-value=1); color coded by MSigDB significantly overlapping genesets (FDR <0.05): KRAS_SHP2 (PID) (red), MYC_Targets_V1 (green), cell cycle (blue), and apoptosis (orange); CCNH (CyclinH); also includes MAPK and TNF signaling. **F**. Differential analysis of PancVH1 vs. HPNE secondary RNAi screen results; preferential lethality (P-value <0.05) and cross reference to KRAS mutant PDAC cell line RNAi screens (JHU) differential with HPNE (red) and PancVH1-HPNE (black).

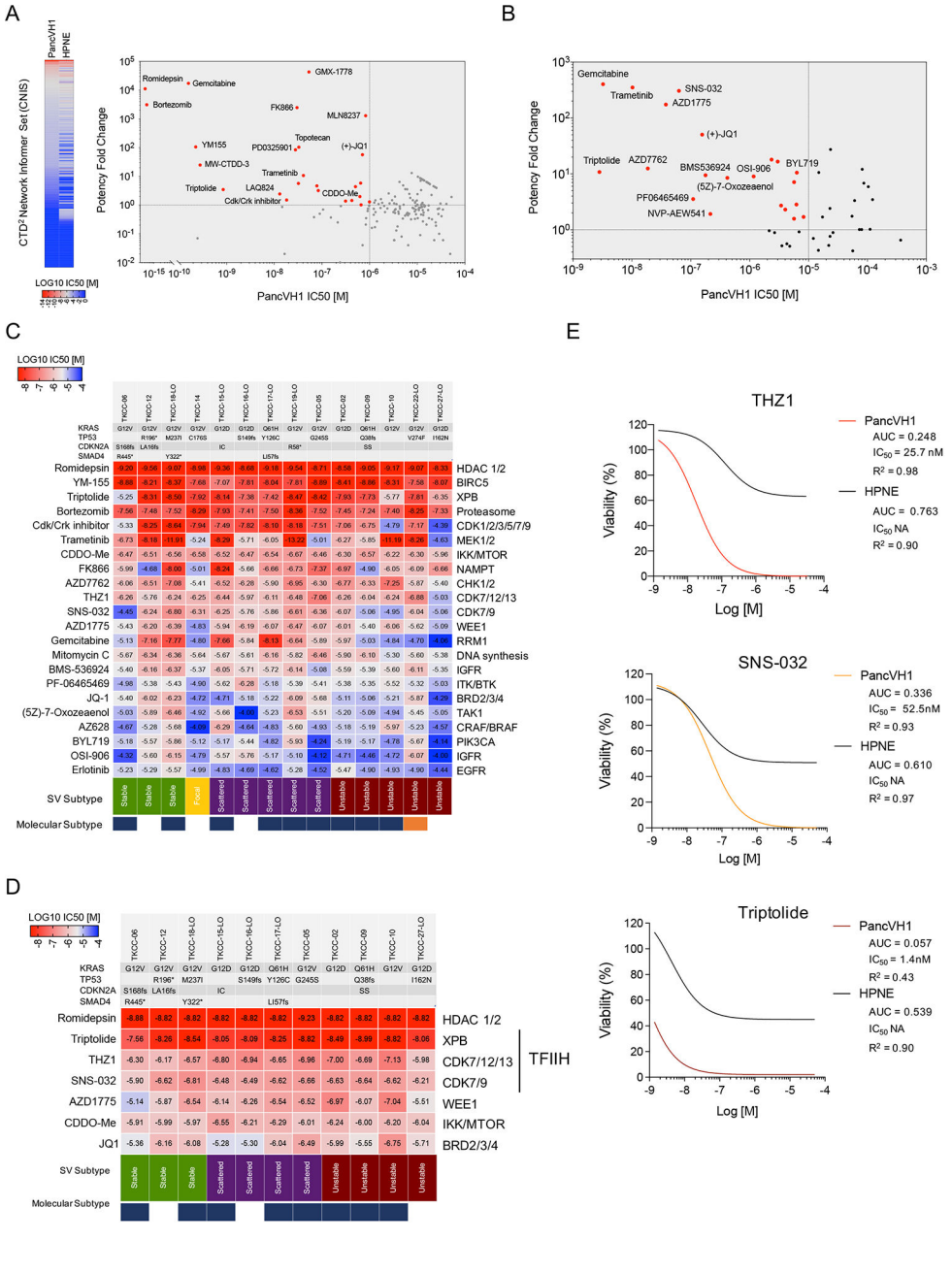


Figure 2

**Figure 2. Drug profiling identifies the TFIIH complex as a potential therapeutic target in KRAS mutant PDAC PDCLs.**

**A**. CNIS drug screen of PancVH1 and HPNE; heatmap of 318 drug sensitivities shown as $\log_{10}$IC50; Bivariate plot of PancVH1 $\log_{10}$IC50 vs. potency fold change ($HPNE_{IC50}$/$PancVH1_{IC50}$); SI Dataset S4A–E. **B**. Bivariate plot of PancVH1 $\log_{10}$IC50 vs. potency fold change ($HPNE_{IC50}$/$PancVH1_{IC50}$) from low-throughput drug screen with 50 selected drugs targeting RNAi targets nominated from druggable genome RNAi screen and associated PDAC biology; SI Dataset S4F–G. **C**. Heatmap of $\log_{10}$IC50 values from fitted dose-response curves of 22 drugs on 14 TKCC PDAC PDCLs; 72hr; 10-point; singleton;

normalized to vehicle (DMSO) condition; AUC values and additional data in SI Dataset S6; TKCC PDCL structural variant (SV) subtypes (Stable, Focal, Scattered, Unstable); molecular subtypes: classical (orange), squamous (blue); and KRAS, TP53, CDKN2A, and SMAD4 status (top) are shown. **D**. Heatmap of $\log_{10}$IC50 values from fitted dose-response curves of 7 drugs including THZ1, SNS-032, and Triptolide on 11 TKCC PDAC PDCLs; 72hr assay; 10-point; 4 technical replicates; normalized to vehicle (DMSO) condition; AUC values and additional data in SI Dataset S6. **E**. Fitted dose response curves of THZ1, SNS-032, and Triptolide on PancVH1 and HPNE cells; 72hr assay; 10-point; 3 technical replicates; range; 50μM −1.4nM; response data are presented as a fitted curve to the mean fractional viability of vehicle condition (DMSO); AUC (area under the curve) values were calculated via trapezoid method with n-parameter logistic regression (nplr); $R^2$ value indicates goodness of fit (0–1).

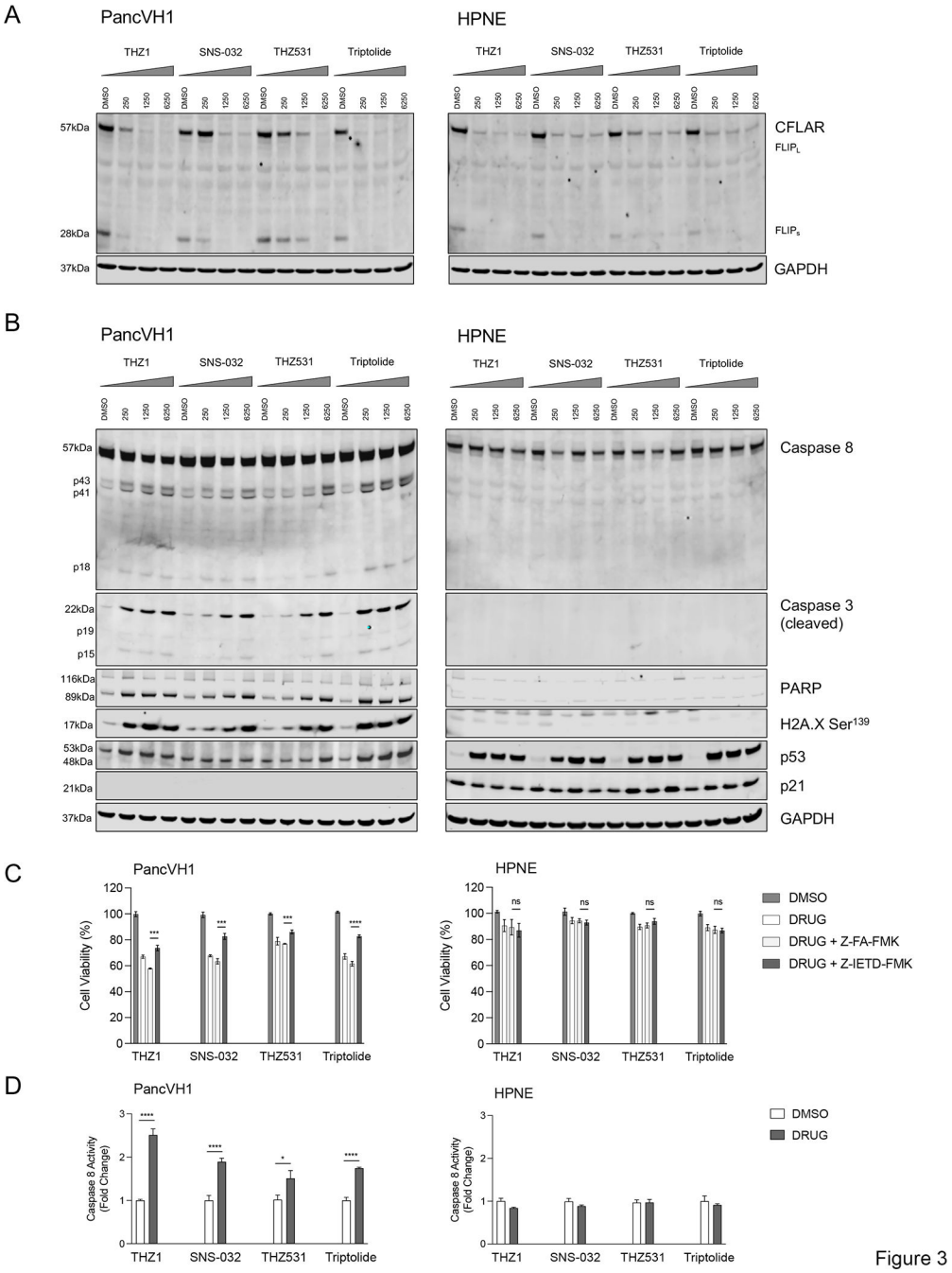


Figure 3

**Figure 3. TFIIH inhibition initiates a CFLAR-mediated caspase-8 dependent apoptotic response in KRAS TP53 mutant PancVH1 PDCL.**

**A.** Immunoblot of dose dependent response to THZ1, SNS-032, THZ531, and Triptolide on CFLAR ($cFLIP_L$ / $cFLIP_S$) expression in PancVH1 and HPNE cells; drug concentrations (nM); 24hr; GAPDH loading control. **B**. Corresponding immunoblot probed for caspase-8, caspase-3 (cleaved), PARP, H2A.X Ser139, p53, and p21; drug concentrations (nM); 24hr; GAPDH loading control. **C.** Caspase-8 inhibition rescues cell death/apoptotic phenotype upon treatment with THZ1, SNS-032, THZ531, and Triptolide in PancVH1 with no significant effect on HPNE; bar graphs of relative cellular viability at 24 hrs post-treatment

with vehicle (solvent), drugs [500nM], drugs with Z-FA-FMK (selective inhibitor of caspases-2,−3,−6,−7 as control), and drugs with Z-IETD-FMK (specific inhibitor of caspase-8); mean ± s.d., n=3; unpaired t-test; significance: ****P<0.0001, ***P<0.001, **P<0.01, *P<0.05**. D**. Caspase-8 activity measured in PancVH1 and HPNE at 24 hrs post-treatment with vehicle (solvent) and THZ1, SNS-032, THZ531, and Triptolide at 500nM; bar graph, mean ± s.d., n=3; unpaired t-test; significance: ****P<0.0001, ***P<0.001, **P<0.01, *P<0.05.

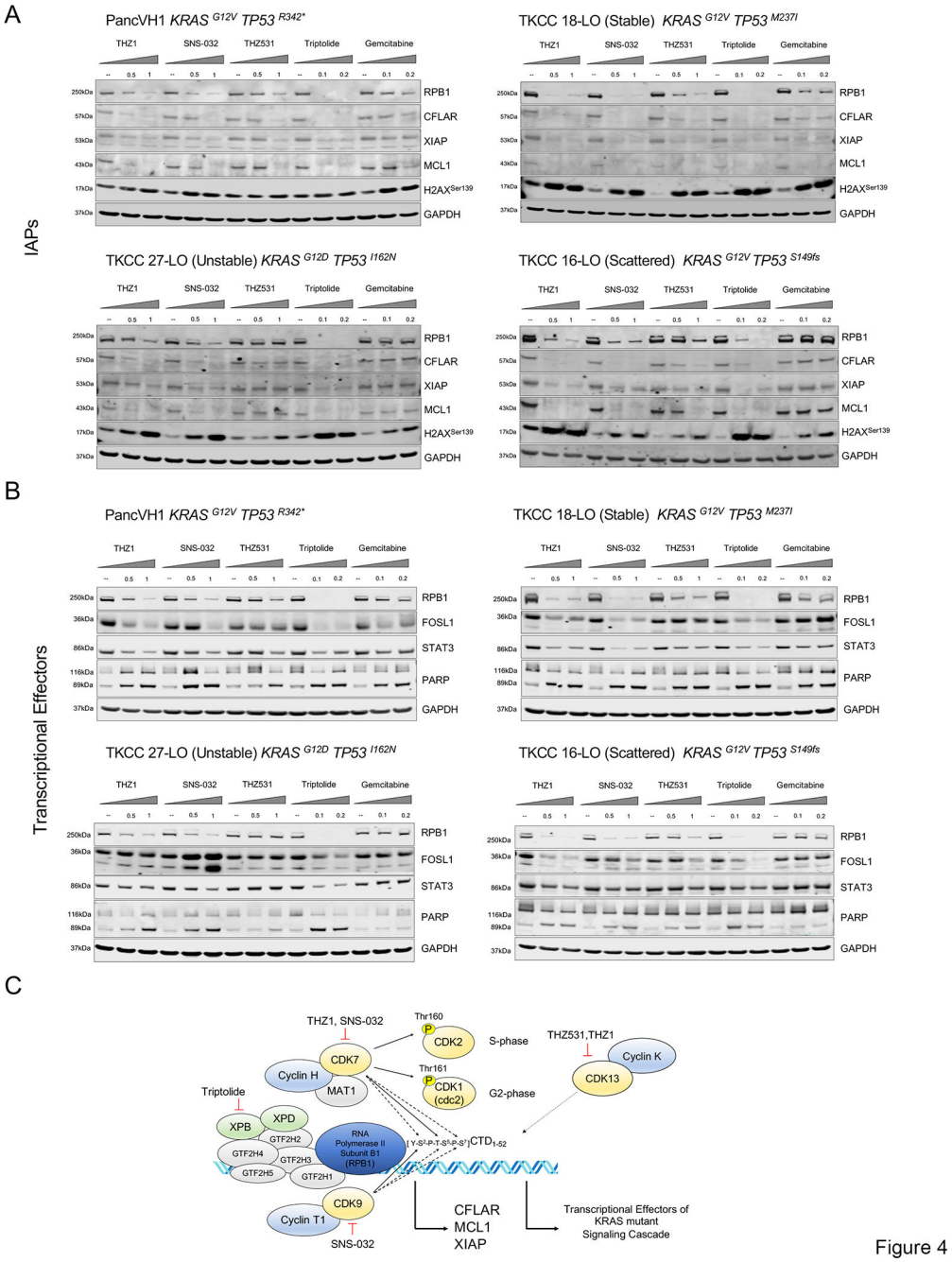


Figure 4

**Figure 4. TFIIH inhibition disrupts the protein stability of RPB1 resulting in the downregulation of IAPs and transcriptional effectors of oncogenic signaling in KRAS TP53 mutant PDCLs.**

**A.** Immunoblots of dose dependent TFIIIH inhibition on the expression of RPB1, CFLAR, and IAPs: MCL1, and XIAP in PDCLs: PancVH1, TKCC18-LO (Stable), TKCC16-LO (Scattered), TKCC27-LO (Unstable); drug concentrations (μM); 24hr; GAPDH loading control. **B.** Immunoblots of dose dependent TFIIIH inhibition on the expression of RPB1, FOSL1, and STAT3 in PDCLs; drug concentrations (μM); 24hr; GAPDH loading control. **C.** Proposed model of TFIIH inhibition on RNA polymerase II transcription. TFIIH complex: GTF2H1 (p62), GTF2H2 (p44), GTF2H3 (p34), GTF2H4 (p52), GTF2H5 (p8),

ATP-dependent DNA helicase subunits XPD (ERCC2), and XPB (ERCC3), and the CAK that includes CDK7, Cyclin H, and MAT1, and inhibition via the covalent CDK7/12/13 inhibitor THZ1, the dual kinase CDK7/CDK9 inhibitor SNS-032, and XPB (subunit of TFIIH) inhibitor Triptolide. In this model, TFIIH inhibition results in the disruption of the spatiotemporal phosphorylation of the RNA polymerase II Subunit B1 carboxy terminal domain (CTD) heptapeptide repeat as well as the stability of the RPB1 protein. RNA polymerase II transcription initiation is therefore arrested leading to the downregulation of CFLAR, IAPs and transcriptional effectors of the KRAS mutant signaling cascade; RPB1 also acts as a substrate for transcriptional kinases CDK9/CyclinT (P-TEFb), essential to RNA polymerase II transcription elongation, and CDK13/CyclinK, involved in the coordination of RNA splicing.

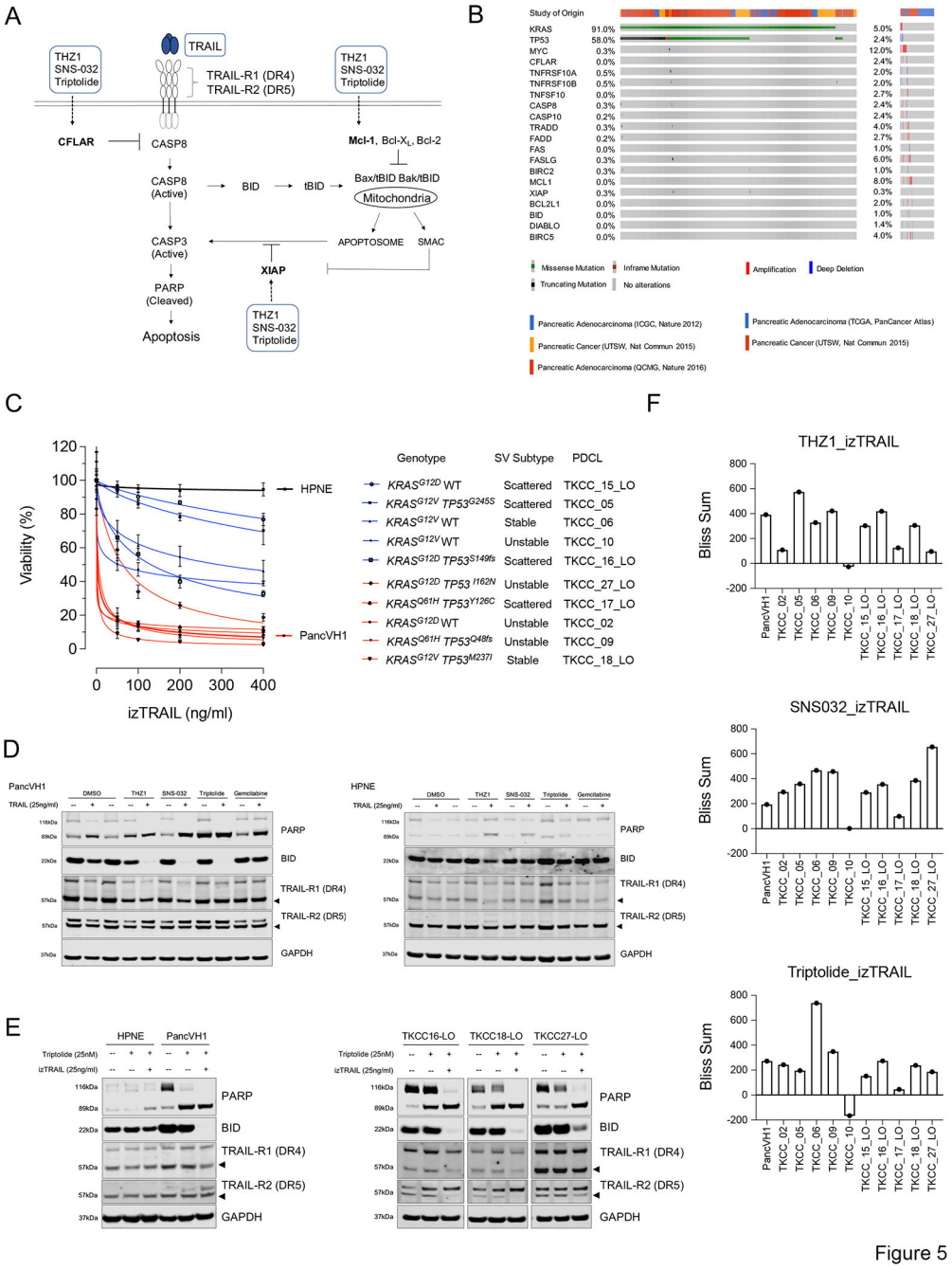


Figure 5

**Figure 5. TRAIL in combination with TFIIH inhibitors demonstrate synergy of response in KRAS mutant PDAC PDCLs.**

**A**. Proposed model for combination therapeutic strategy where TFIIH/RPB1 inhibition decreases the expression of CFLAR, the negative regulator that competes with caspase-8 for binding to the death inducing signaling complex (DISC) and inhibits the execution of the extrinsic apoptotic pathway. TFIIH inhibition also decreases expression of IAPs MCL1 and XIAP, both with key roles in the execution of mitochondrial-mediated apoptosis. In this model, TRAIL could potentially synergize with TFIIH inhibition to optimize the extrinsic and intrinsic mitochondrial-mediated apoptotic pathway in KRAS mutant PDAC. **B**. Public

datasets (QCMG, ICGC, UTSW) genomic data on PDAC patients (cBioPortal). **C**. izTRAIL dose response curves on KRAS mutant PDCLs and HPNE; izTRAIL concentrations range (0–400 ng/ml); fitted dose response curve, nonlinear regression; PDCL izTRAIL sensitivity divided into two groups (red < 50% at 100ng/ml < blue). HPNE cell line (black). **D.** Immunoblot of combination treatment with TFIIH inhibitors (THZ1 (500nM), SNS-032 (500nM), Triptolide (25nM)) and izTRAIL(25 ng/ml); 24hr assay; PARP, BID, TRAIL-R1 (DR4), TRAIL-R2 (DR5) expression via immunoblot in both PancVH1 and HPNE; GAPDH loading control; vehicle (DMSO); gemcitabine (25nM). **E.** Immunoblot of combination treatment with izTRAIL(25ng/ml) and TFIIH inhibitor Triptolide (25nM); 24hr assay; PARP, BID, TRAIL-R1 (DR4), and TRAIL-R2 (DR5) protein expression in PDCLs; GAPDH loading control. **F**. Bar graphs of Bliss sum demonstrating drug synergy of response to TFIIH inhibition (THZ1, SNS-032, and Triptolide) in combination with izTRAIL in KRAS mutant PDCLs (10/11); 72 hr post-treatment assay endpoint; Bliss sum calculated by excess over Bliss independence model across the combination matrix: synergistic>0, additive=0, antagonistic <0.